Three conserved hydrophobic residues in the α2 helix of the Pit CC domain contribute to its plasma membrane localization and immune induction

Qiong Wang[1, 2, $], Yuying Li[2, 3, $], Ken-ichi Kosami[2, 4, $], Chaochao Liu[5], Jing Li[2, 6], Dan Zhang[1], Daisuke Miki[2], and Yoji Kawano[2, 7, 8]

[1] School of Horticulture and Plant Protection, Yangzhou University, Yangzhou 225009, China

[2] CAS Center for Excellence in Molecular Plant Sciences, Shanghai Center for Plant Stress Biology, Chinese Academy of Sciences, Shanghai 201602, China

[3] Lingnan Guangdong Laboratory of Modern Agriculture, Genome Analysis Laboratory of the Ministry of Agriculture, Agricultural Genomics Institute at Shenzhen, Chinese Academy of Agricultural Sciences, Shenzhen 440307, China

[4] Fruit Tree Research Center, Ehime Research Institute of Agriculture, Forestry and Fisheries, Ehime 791-0112, Japan

[5] School of Biotechnology, Jiangsu University of Science and Technology, Zhenjiang 212021, China

[6] University of Chinese Academy of Sciences, Beijing 100049, China

[7] Kihara Institute for Biological Research, Yokohama City University, Kanagawa 244-0813, Japan

[8] Institute of Plant Science and Resources, Okayama University, Okayama 710-0046, Japan

[$] These authors contributed equally to this work.

Correspondence should be addressed to Yoji Kawano,

Institute of Plant Science and Resources

Okayama University

2-20-1, Chuo, Kurashiki, Okayama 710-0046, Japan

Tel: +81-86-434-1242

E-mail: yoji.kawano@okayama-u.ac.jp

Author emails:

Qiong Wang: wangqiong@yzu.edu.cn

Yuying Li: liyuying@caas.cn

Ken-ichi Kosami: kenichi.kosami.1985@gmail.com

Chaochao Liu: qdliuchaohi@163.com

Jing Li: jingli@psc.ac.cn

Dan Zhang: MZ120201287@yzu.edu.cn

Daisuke Miki: miki@sibs.ac.cn

Yoji Kawano: yoji.kawano@okayama-u.ac.jp

ABSTRACT

Nucleotide-binding leucine-rich repeat (NLR) proteins work as crucial intracellular immune receptors. N-terminal domains of NLRs fall into two groups, namely coiled-coil (CC) and Toll-interleukin 1 receptor (TIR) domains, which play critical roles in signal transduction and disease resistance. However, the activation mechanisms of NLRs, and how their N-termini are involved in immune induction, remain largely unknown. Here, we revealed that the rice NLR Pit self-associates through its CC domain. The α2 helix of the Pit CC domain possesses three conserved hydrophobic residues that are known to be involved in oligomer formation in two NLRs, barley MLA10 and Arabidopsis RPM1. Interestingly, the function of these residues in Pit is different from that in MLA10 and RPM1. Although the three hydrophobic residues are important for Pit-induced disease resistance against rice blast fungus, they do not participate in self-association or in binding to downstream signaling molecules. Based on homology modeling of Pit using the structure of the Arabidopsis NLR ZAR1, we tried to clarify the role of the three conserved hydrophobic residues and found that they are involved in the plasma membrane localization. Our findings provide novel insights for understanding the mechanisms of NLR activation as well as the relationship between subcellular localization and immune induction.

Key words: NLR protein; plasma membrane localization; self-association; effector-triggered immunity; rice

INTRODUCTION

Plants have developed two tiers in their immune system, called pattern-triggered immunity (PTI) and effector-triggered immunity (ETI), to detect invasion by various pathogens (Dodds and Rathjen, 2010; Zhou and Zhang, 2020). The initiation of PTI depends on the successful perception of conserved pathogen-associated molecular patterns (PAMPs) by surface-localized pattern recognition receptors (PRRs) (Macho and Zipfel, 2014; Noman et al., 2019). Once PTI signaling is activated, it is usually accompanied by a series of immune responses, such as the production of reactive oxygen species (ROS), the expression of pathogenesis-related genes, and the synthesis of antimicrobial phytoalexins and the cell wall component lignin (Bigeard et al., 2015). In general, PTI is sufficient to resist the attack of pathogens. Nevertheless, pathogens have acquired the ability to secrete effectors into the apoplast or the plant cytoplasm to counteract the defense of PTI (Ma et al., 2018). To overcome this invasion, plants have developed ETI as the second tier of the immune system (Cui et al., 2015). The majority of genetically characterized disease resistance traits in plants map to genes encoding nucleotide-binding domain and leucine-rich repeat proteins (NLRs). These act as receptors to surveil effectors derived from pathogens and to activate ETI, which includes the hypersensitive response (HR) and ROS production. NLRs share two core domains: a central nucleotide-binding (NB-ARC) domain and a C-terminal leucine-rich repeat (LRR) domain (Cui et al., 2015). The NB-ARC domain is thought to serve as a switch domain in NLRs by controlling nucleotide exchange and hydrolysis, and this nucleotide exchange leads to conformational change and oligomerization of NLRs, resulting in the triggering of ETI (Takken et al., 2006). Highly variable LRR domains define at least part of the recognition specificity of NLRs to pathogen effector proteins. The N-terminus of NLRs is categorized into two domains, namely a Toll/interleukin-1 receptor (TIR) domain and a coiled-coil (CC) domain, and therefore NLRs are subclassified into TIR-NLRs (TNLs) and CC-NLRs (CNLs). Previous studies have demonstrated that in several NLRs, overexpression of the CC or TIR domain alone has autoactivity to induce cell death, implying that N-terminal CC and TIR domains are important platforms to trigger immune responses (Bernoux et al.,

2011; Collier et al., 2011; Maekawa et al., 2011; Swiderski et al., 2009; Wang et al., 2015). N-terminal CC and TIR domains are now known to play key roles in several functions, including indirect surveillance of pathogen effectors and binding of downstream signaling molecules (Jones et al., 2016; Kourelis and van der Hoorn, 2018; Wang et al., 2021).

Moreover, self (homomers) and non-self (heteromers) oligomerization of N-terminal NLRs are indispensable to trigger ETI (Maekawa et al., 2011; Wang et al., 2019a; Williams et al., 2014; Wroblewski et al., 2018). Structural studies have revealed that TIR domains exhibit a flavodoxin-like fold consisting of five α-helices surrounding a five-strand β-sheet, and at least two different oligomerization interfaces exist among the TIR domains (Chakraborty and Ghosh, 2020). The first structure of the CC domain of CNL was revealed as an antiparallel homodimer of barley MLA10 in crystals (Maekawa et al., 2011). Subsequent studies have proved the CC domains of all the other NLRs including wheat Sr33 and potato Rx behave monomeric proteins with a four-helix bundle conformation (Casey et al., 2016; Hao et al., 2013). Recently, using a cryo-EM, Wang et al. revealed the full length structures of the Arabidopsis CNL ZAR1 in monomeric inactive and transition states as well as the active pentameric ZAR1 resistosome (Wang et al., 2019a). The CC domain of ZAR1 also displays a four-helix bundle conformation. A large portion of the helix α1 (residues 12–44) of the MLA10 CC domain appears to be an important interface for homodimerization. Single mutations in three hydrophobic residues (I33, L36, and M43) of the helix α1 in MLA10 dramatically decreased self-association as well as binding activity to a downstream signaling molecule, HvWRKY1, resulting in compromised resistance to the pathogenic powdery mildew fungus (Maekawa et al., 2011). The hydrophobicity of these residues is conserved among various CNLs including Arabidopsis RPM1. Triple mutation of the corresponding three hydrophobic residues in RPM1 also leads to a loss of self-association and immune induction activity (El Kasmi et al., 2017). All of the single mutants in three hydrophobic residues show reduced interaction with the small host protein RIN4 (El Kasmi et al., 2017). It is unclear whether these residues are universally involved in self-association or whether their functions differ in each NLR.

Evidence has been accumulating that the subcellular distribution of NLRs is important for their functions. Perception of the fungal effector AVR_{A10} by MLA10 triggers the nuclear translocation from the cytosol, resulting in interaction between MLA10 and HvWRKY1 in the nucleus to induce defense responses (Shen et al., 2007). Bacterial effector AvrRps4 targets distinct branches of nucleus/cytoplasm-accumulated RPS4-EDS1 immune complex to coordinate host defense (Heidrich et al., 2011). The potato CNL Rx1 is located in both the cytoplasm and the nucleus, and the appropriate nucleocytoplasmic distribution of Rx1 is required for full functionality (Slootweg et al., 2010; Tameling et al., 2010). Rx1 activation triggered by effector recognition occurs only in the cytoplasm. The CC domain and the cochaperone SGT contribute to nuclear localization of Rx1, but the LRR domain is associated with cytoplasmic localization. The Arabidopsis CNL RPM1 requires plasma membrane distribution while the potato CNL R3a needs endomembrane localization, and disrupting the proper localization of both NLRs impairs their functions (Engelhardt et al., 2012; Gao et al., 2011). The oligomerization-induced active Arabidopsis ZAR1 complex associates with the plasma membrane (Wang et al., 2019a). Although our knowledge of NLR protein localization has increased in recent years, it is not yet sufficient to understand the mechanisms and significance of the dynamic nature of NLR protein localization or the relationship between subcellular localization and activation states.

We have previously revealed that the small GTPase OsRac1 functions as a molecular switch in rice and plays key roles in both PTI and ETI (Akamatsu et al., 2013; Kawano et al., 2010; Kawano et al., 2014b; Kawano and Shimamoto, 2013). OsRac1 forms immune protein complex(es) directly or indirectly with 16 binding partners such as NADPH oxidase and OsMPK6, thereby leading to the induction of immune responses (Akamatsu et al., 2013; Chen et al., 2010; Kawano et al., 2014b; Kawano and Shimamoto, 2013; Kosami et al., 2014; Lieberherr et al., 2005). OsRac1 acts as a downstream switch molecule for three CNLs, Pit, Pia, and PID3, which all confer resistance to *Magnaporthe oryzae*, implying that OsRac1 is a key signaling switch for rice CNLs (Kawano et al., 2010; Ono et al., 2001; Wang et al., 2018; Zhou et al., 2019). Recently, we clarified how the CNL Pit activates OsRac1. Pit interacts directly with the

GDP/GTP exchanger (GEF) protein OsSPK1, which is an activator for OsRac1, through its CC domain (Wang et al., 2018) and also associates with OsRac1 through its NB-ARC domain (Kawano et al., 2010). Both Pit and OsRac1 seem to be posttranslationally modified by a lipid modification, palmitoylation, and these three proteins may form a ternary complex at the plasma membrane to trigger ETI (Kawano et al., 2014a; Ono et al., 2001; Wang et al., 2018; Yalovsky, 2015).

In this study, we clarified the role of the above-mentioned three conserved hydrophobic residues (I34, L37 and L41) which are located in the α-helix 2 of the CC domain of Pit. Interestingly, the three residues are involved in the plasma membrane localization of Pit, and are indispensable for Pit-mediated disease resistance to rice blast fungus, but do not participate in self-association and binding to its direct signaling molecules OsSPK1 and OsRac1. We revealed that the property of Pit contrasts partly with that of the previosly reported MLA10 and RPM1 (Maekawa et al., 2011; Kasmi et al., 2017). Adachi et al. found the consensus sequence called MADA motif in the N-termini of various CNLs which matches the important residues in the N-terminal α-helix 1 of ZAR1 (Adachi et al., 2019). This MADA motif exists in only ~20% of CC-type NLRs. Collectively, our results shed light on similarities and differences in the mode action of CC domains of NLRs.

RESULTS

Pit self-associates through its CC domain

Since several CNL and TNL proteins have been reported to self-associate (Ade et al., 2007; Mestre and Baulcombe, 2006), we tested whether the rice NLR Pit forms oligomers *in planta*. We transiently co-expressed full-length Pit WT-HA and Pit WT-Myc in *Nicotiana benthamiana* and performed a co-immunoprecipitation (co-IP) assay. When Pit WT-HA was precipitated with anti-HA antibody, Pit WT-Myc co-precipitated but a control GUS-HA did not, indicating that Pit self-associates *in planta* (Figure 1A). Previous studies have demonstrated that the N-terminal CC and TIR domains are important interfaces for oligomerization in NLRs, and that these interactions are indispensable for NLR functions (Maekawa et al., 2011; Williams et al., 2014). Since the overexpression CC domain of some NLRs sufficiently induce cell death (Wang et al., 2021), we overexpressed several CC domain deletion mutants of Pit including Pit 1-140 aa which is equivalent to the minimal cell death induction region of MLA10 1-142 aa, Sr33 1-142 aa, and Sr50 1-145 aa in *N. benthamiana* but all of them failed to induce cell death (Figures S1A, S1B, and S1C), indicating Pit CC domain is not sufficient to induce cell death. It appears that not all the CC domains of NLRs have cell death activity because the expression of the CC domains of RPM1 (El Kasmi et al., 2017), Rx (Rairdan et al., 2008), RPS5 (Ade et al., 2007), Pm60 (Zou et al., 2018), and Sr35 (Bolus et al., 2020) also do not elicit cell death. Next, we examined whether Pit self-associates through its CC domain. By using a yeast two-hybrid assay, we found that the CC domain of Pit formed oligomers (Figure 1B). Consistent with this observation, self-association between the CC domains of Pit was observed in a co-IP assay in *N. benthamiana* (Figure 1C) and an *in vitro* binding assay (Figure 1D). Taken together, these results indicate that the CC domain contributes to Pit oligomerization.

Three conserved residues do not contribute to self-association of Pit

Although the primary sequences of the N-terminal CC domain of NLRs are dissimilar, three hydrophobic residues (I33, L36, and M43) of the helix α1 in MLA10 are highly conserved among the known CNL proteins including Pit (Maekawa et al., 2011) (Figure

2A). In MLA10 and RPM1, these three residues are involved in self-association and are indispensable for immune induction (El Kasmi et al., 2017; Maekawa et al., 2011). I33, L36, and M43 in MLA10 correspond to I34, L37, and L41 in Pit. Our finding that Pit forms oligomers through its CC domain raised the possibility that the three conserved hydrophobic residues of Pit also participate in oligomerization and are essential for its function. To test this hypothesis, we built a homology model of the CC domain of Pit using the crystal structure of the CC domain of MLA10 . Similar to MLA10, the structure model of the CC domain of Pit dimerized through the helix α1 using three hydrophobic residues of I34, L37, and L41 (Figure 2B). We generated CC domain Pit mutants in which these three conserved residues were converted to negatively charged glutamic acid, and tested whether they are involved in self-association. Interestingly, both the single mutations (Pit I34, L37, or L41) and the triple mutation of Pit (Pit 3E: Pit I34E L37E L41E) retained self-association ability in an *in vitro* binding assay (Figure 2C), and a consistent result was obtained in a yeast two-hybrid assay (Figures 2D and S2A). We also conducted a co-IP assay in *N. benthamiana* using full-length Pit but could not observe a visible effect on self-association (Figure 2E). Overall, these results indicate that the three hydrophobic residues are not essential for self-association of Pit.

Mutations in the three conserved residues of Pit compromise Pit-mediated immune responses

Next, we examined whether the effects of the hydrophobic residue mutants of Pit influenced immune responses. We have previously generated a constitutively active form of Pit, named Pit D485V. Pit D485V is a MHD motif mutant that is able to induce cell death and ROS production in *N. benthamiana*, probably through the employment of tobacco orthologs of OsRac1 and OsSPK1 as downstream signal transducers because the overexpression of the dominat negative form of OsRac1 suppresses Pit D485V-induced cell death in *N. benthamiana* (Kawano et al., 2010; Kawano et al., 2014b). The single mutations and the triple mutation in the three hydrophobic residues clearly attenuated Pit D485V-induced cell death (Figures 3A and S2C) and ROS production

(Figures 3B, S2B and S2C). We also employed two rice systems to evaluate the Pit mutants. We used a luciferase reporter system to monitor the effect of the Pit mutants on cell death in rice protoplasts. In this system, we transfected the *Pit* mutants with a *luciferase* vector into rice protoplasts and measured the viability of protoplasts based on luminescence. We found that the luciferase activity in cells expressing Pit WT was significantly lower than that in cells expressing control GUS, indicating that Pit WT is autoactive and induces cell death in rice protoplasts (Figure 3C). This Pit WT-induced cell death was abolished by the introduction of the mutations in three conserved hydrophobic residues (Figures 3C and S2D). Next, we tested the effect of the hydrophobic residue mutants of Pit on disease resistance to rice blast fungus. In this experiment, we generated transgenic plants of the susceptible rice cultivar Nipponbare carrying the exogenous *Pit* resistance genes (Figure S3A), and chose the avirulent rice blast fungus *M. oryzae* race 007.0, because Pit-dependent disease resistance has been established between *Pit* and *M. oryzae* race 007.0 (Hayashi et al., 2010). Therefore, Nipponbare is a suitable cultivar to assess transgenes encoding the *Pit* mutants. Nipponbare expressing *Pit* WT displayed shorter lesions induced by *M. oryzae* than did Nipponbare, but this effect was compromised in both single and triple mutants for the three hydrophobic residues (Figures 3D and 3E). We also quantified fungal invasion by measuring the amount of fungal DNA using real-time PCR (Figure 3F). The result of this qPCR was consistent with that of the lesion length comparison, showing that mutation of the three hydrophobic residues perturbed Pit-triggered resistance to avirulent rice blast fungus. Take together, these data indicate that the three hydrophobic residues in the CC domain of Pit are indispensable for Pit-mediated immune responses.

Mutations in the three conserved hydrophobic residues abolish Pit-induced OsRac1 activation but do not affect the interaction with OsRac1 and OsSPK1

Since the three hydrophobic residue mutations of Pit significantly perturbed Pit-mediated immune responses (Figure 3), we checked the interactions between Pit and its two downstream signaling molecules: the molecular switch of rice immunity OsRac1 and its activator OsSPK1 . Pit may form a ternary complex with OsSPK1 and OsRac1

at the plasma membrane and activates OsRac1 through OsSPK1 to induce Pit-mediated immunity (Kawano et al., 2010; Wang et al., 2018). We previously mapped the binding region of OsSKP1 in Pit and revealed that a proline-rich motif of the CC domain in Pit (residues 91–95) is required for its binding to OsSPK1 (Wang et al., 2018). Consistent with that finding, there is no visible effect in any of the three hydrophobic residue mutants of Pit on binding to OsSPK1 in a co-IP assay in *N. benthamiana* using the CC domain (Figure 4A) and an *in vitro* binding assay (Figure S3B) and the full-length polypeptide (Figure S3C) of Pit. Moreover, mutating the three hydrophobic residues of Pit did not change its binding activity to OsRac1, probably because OsRac1 binds to the NB-ARC domain of Pit (Figure 4B) (Kawano et al., 2010). Next, we checked OsRac1 activation by the Pit mutants using a Förster resonance energy transfer (FRET) sensor called Ras and interacting protein chimeric unit (Raichu)-OsRac1 (Wong et al., 2018). In this sensor, intramolecular binding of the active GTP-OsRac1 to CRIB brings CFP closer to Venus, enabling FRET from CFP to Venus when OsRac1 is activated (Wong et al., 2018). The resulting Venus fluorescence represents the activation state of OsRac1 *in vivo*: low and high ratios of Venus/CFP fluorescence correspond to low and high levels of OsRac1 activation, respectively. The ratio of Venus/CFP fluorescence of Raichu-OsRac1 in rice protoplasts expressing Pit D485V was much higher than that in protoplasts expressing a control GUS, indicating that Pit D485V activates OsRac1 in rice protoplasts, but the triple mutant Pit 3E with the D485V mutation failed to trigger this activity (Figures 4C and 4D). Thus, we conclude that Pit 3E retains binding activity to OsSPK1 and OsRac1 but loses the ability of wild-type Pit to trigger OsRac1 activation.

Homology modeling of Pit

From the results of our interaction studies in Figure 2, it appears that the MLA10 structure is not applicable to Pit. The reported structures of the CC domain of NLRs resolve into two types: 1) MLA10 forms dimers and shows a helix–loop–helix structure (Maekawa et al., 2011), 2) while Sr33 and Rx display a distinct structure that exhibits a four-helix bundle (Casey et al., 2016; Hao et al., 2013). Recently, Wang et al. solved

the structure of the inactive and active states of the full-length CNL ZAR1, which revealed that the N-terminal CC domain of inactivated ZAR1 (PDB code 6J5W, Chain A, 1–113) possesses a four-helix bundle, like Sr33 (PDB code 2NCG) and Rx (PDB code 4M70, Chain A) (Figure 5A), implying that Pit also displays the four-helix bundle (Casey et al., 2016; Hao et al., 2013; Wang et al., 2019b). To test this hypothesis and understand the function of I34, L37, and L41 in Pit, we undertook detailed homology structure modeling of Pit based on the inactive (ADP-bound) and active (dATP-bound) structures of the NLR ZAR1 (Wang et al., 2019a; Wang et al., 2019b). The structure model of the CC domain of Pit displays a four-helix bundle, and the three hydrophobic residues are buried inside the CC domain (Figure 5B). These residues locate on α-helix 2 (α2) and make hydrophobic contact with α-helix1 (α1) and α-helix 3 (α3), which may enhance the stability of the four-helix bundle. The three hydrophobic residues are conserved in Sr33 (I33, L36, and L40), Rx (L24, F27, and L31), and ZAR1 (L31, L34, and L38), and they also form similar hydrophobic contacts (Casey et al., 2016; El Kasmi et al., 2017) (Figure 5B). In the structure model of Pit based on the inactive ZAR1, the LRR domain sequesters Pit in a monomeric state (Figure 5C). The CC domain of Pit contacts the helical domain (HD1) and a winged-helix domain (WHD) in the NB-ARC domain, and these interactions may keep the CC domain inactive (Burdett et al., 2019; Wang et al., 2019b).

ZAR1 transitions from a monomeric inactive form to the active form, a wheel-like pentameric resistosome, during immune activation (Wang et al., 2019a; Wang et al., 2019b). Since Pit forms oligomers (Figure 1), we also generated a structure model of Pit with reference to the structure of the active form of ZAR1 (Wang et al., 2019a). Superposition of the Pit structure model with one protomer of Pit structure model based on the inactive ZAR1 revealed that the conformational change between the active and inactive forms of Pit probably occurs at two regions: around the hinge linking the HD and WHD domains, and in the α1 helix of the CC domain (Figure S4A). In the Pit structure model based on the active ZAR1, Pit forms a wheel-like pentamer and all the subdomains of Pit are involved in this oligomerization (Figure S4B). The formation of an α-helical funnel-shaped structure in the CC domain contributes to the

oligomerization of Pit and is consistent with the self-association of Pit through its CC domain (Figures 1 and S4B) (Wang et al., 2019a). Interestingly, the three conserved hydrophobic residues make hydrophobic contacts with V75, I78, and V79 of the α3 helix, which itself forms hydrophobic interactions with isoleucines I500 and L510 in the WHD domain (Figure S4C). We also found that L31 and L34 of the α2 helix make hydrophobic contacts with I75 and L76 of the α3 helix, and L115 and I118 of the α4 helix (Figure S4D), which appear to provide a foundation when the activated protein oligomerizes via its CC domain to form a functional oligomer. These structural features of ZAR1 are similar to those of Pit modeling.

Mutations in the three hydrophobic residues of Pit perturb its plasma membrane localization

Next, we checked the localization of the hydrophobic residue mutants of Pit in rice protoplasts. We had previously demonstrated that Pit WT is localized at the plasma membrane, but we now found that introducing single mutations into the three hydrophobic residues compromised Pit's plasma membrane localization (Figure 6A) (Kawano et al., 2010; Kawano et al., 2014a). We further investigated the localization of the hydrophobic residue mutants in *N. benthamiana* and found that Pit WT was well merged with FM4-64, a plasma membrane marker, confirming that Pit WT is localized in the plasma membrane; in contrast, plasma membrane localization was disrupted in all of the hydrophobic residue mutants (Figure 6B). In addition, we transiently expressed Myc-tagged Pit variants in *N. benthamiana* and roughly fractionated the total proteins of tobacco leaves into two compartments: soluble (S) and membrane (M) fractions. Consistently, the membrane accumulation in the three Pit mutants, I34E, L37E and L41E, was significantly decreased compared with that in Pit WT (Figure 6C). Taken together, these results indicate that the three conserved hydrophobic residues of Pit are required for its proper plasma membrane localization.

We checked the OsSPK1-binding activity of these Pit mutants by bimolecular fluorescence complementation (BiFC) assay in *N. benthamiana*. Consistent with the results of the binding assays (Figure 4A and 4B), OsSPK1 binding was comparable in

the mutants to that in Pit WT (Figure S5A). However, the localization of the Pit–OsSPK1 complex differed between Pit WT and the hydrophobic mutants. Pit WT interacted with OsSPK1 at the plasma membrane, as reported previously (Figure S5A) (Wang et al., 2018), but a large proportion of the complexes between OsSPK1 and the Pit mutants was mislocalized away from the plasma membrane. Finally, we examined complex formation between OsRac1 and the Pit mutants by a BiFC assay and found that the Pit WT-OsRac1 complex was situated at the plasma membrane. Interestingly, none of the mutations in the hydrophobic residues disrupted the Pit-OsRac1 interaction at the plasma membrane (Figure S5B), probably because OsRac1 is anchored there by its lipid modification. Taken together, these results indicate that the three conserved hydrophobic residues of Pit are required for its plasma membrane localization.

DISCUSSION

Several TNLs and CNLs have been reported to self-associate through their N-terminal CC or TIR domains; hence, self-association via their N-termini appears to be a general feature of NLRs (Ade et al., 2007; El Kasmi et al., 2017; Maekawa et al., 2011). Here, we found that the rice blast resistance protein Pit also self-associates through at least its CC domain (Figure 1). Full-length Pit forms oligomers in the absence of a pathogen effector, suggesting that it may self-associate before activation and behave like other NLRs, such as RPM1, RPS5, and MLA (Ade et al., 2007; El Kasmi et al., 2017). Previous biophysical analyses have shown that MLA10 is a monomer in solutions but has a dimeric helix-loop-helix structure in crystals (Casey et al., 2016; Maekawa et al., 2011). It is possible that the dimeric helix-loop-helix structure of MLA10 occurs under the special condition because MLA10 is predominantly monomeric in solution and its character in solution is different from that in the crystals (Bentham et al., 2018; Burdett et al., 2019; Casey et al., 2016). Moreover, the CC domain structures of all other NLRs, including Rx, Sr33, and ZAR1, exhibit a four-helix bundle structure (Casey et al., 2016; El Kasmi et al., 2017; Wang et al., 2019a). Single mutations in the hydrophobic residues (I33, L36, and M43) of α1 helix of MLA10 markedly suppressed self-association, resulting in compromised resistance to *Blumeria graminis* f. sp. *hordei*. We found that

introducing the single and triple mutations into Pit did not affect oligomer formation, indicating that these residues make at most a marginal contribution to self-association (Figure 2). In the Pit structure model based on the active ZAR1, I34, L37, and L41 are located on the α2 helix and are buried inside the CC domain, implying that they do not contribute to self-association of the CC domain. This structure model also fits well with the results of our binding assays (Figure 2). In addition, it is possible that Pit displays a four-helix bundle structure, similar to other NLRs such as Rx, Sr33, and ZAR1. We attempted to clarify the structure of the CC domain of Pit and produced an expression system for the CC domain and full-length Pit protein using *E. coli* and insect cells, but we were unable to obtain intact Pit proteins due to difficulties in expression. The structural analysis of the Pit CC domain will be a topic for future research.

Several CNLs, including RPM1 (Gao et al., 2011), RPS2 (Axtell and Staskawicz, 2003), RPS5 (Qi et al., 2012), and Tm-2^2 (Chen et al., 2017), have been reported to be localized in the plasma membrane, and this localization is indispensable for their immune induction. RPM1 appears to anchor to the plasma membrane through the plant guardee protein RIN4, which is localized to the membrane via palmitoylation (Kim et al., 2005). Two lipid modifications, myristoylation, and palmitoylation, in the CC domain of RPS5, participate in its plasma localization, protein stability, and function in an additive manner. We have previously revealed that a free N-terminus of Pit is required for its function because the N-terminal fusion of GFP compromises cell death activity (Kawano et al., 2014a). Consistent with this, Pit has two palmitoylation sites in its CC domain, which play a key role in the plasma membrane localization of Pit (Kawano et al., 2014a). The resting Pit is localized exclusively in the plasma membrane (Figure 6) (Kawano et al., 2014a), indicating that plasma membrane localization alone is not sufficient to trigger activation. The plasma membrane localization of Pit is ATP-binding activity-dependent because the P-loop mutant of Pit K203R is mislocalized (Kawano et al., 2010). This feature is similar to other CNLs, including RPM1, TM-22, and RPS5, whose auto active mutants are primarily localized to the plasma membrane (Chen et al., 2017; El Kasmi et al., 2017; Qi et al., 2012).

Recently, the structures of active and inactive forms of ZAR1 have been reported, revealing a more detailed structural observation of the NLR protein. Inactive ZAR1 forms a monomeric complex with resistance-related kinase (RKS1). *Xanthomonas campestris* pv. *campestris* AvrAC uridylates the PBS1-like protein 2 (PBL2) kinase to produce PBL2UMP, which triggers the pentameric ZAR1–RKS1–PBL2UMP resistosome *in vitro* and *in vivo* (Hu et al., 2020; Wang et al., 2019a; Wang et al., 2019b). Resistosome formation is required for AvrAC-triggered cell death and disease resistance. The *Pseudomonas syringae* effector HopZ1a also induces the oligomerization of ZAR1 *in vivo* (Hu et al., 2020). During the transition from the inactive to the active states of ZAR1, positional translation through unfolding and refolding in the a4 helix allows the α1 helix to be released from the four-helix bundle (Wang et al., 2019a). This conformational change of the α1 helix leads to the pentameric funnel-shaped structure of the CC domain of ZAR1. The funnel-shaped structure of active ZAR1 is similar to previously characterized pore-forming proteins, such as mixed lineage kinase-like (MLKL) and hemolytic actinoporin fragaceatoxin C (FraC) (Tanaka et al., 2015). Notably, FraC showed a similar conformational change during pore formation to that upon the activation of ZAR1. The N-terminal helix of FraC is released from the monomer and is capable of forming a funnel-shaped octamer, leading to its insertion into the cell membrane. The structure of the ZAR1 oligomer implies that the funnel structure of the CC domain of the ZAR1 oligomer also inserts into the cell membrane and induces cell death (Wang et al., 2019a). It appears that a funnel-shaped structure participates in membrane localization (Adachi et al., 2019). Recently, Adachi et al. found the consensus sequence called MADA motif in the N-termini of various CNLs which matches the N-terminal α1 helix of ZAR1. They predicted three residues mapped to the outer surface of the funnel-shaped structure of NRC4 based on the ZAR1 resistosome structure and substituted these three hydrophobic residues for negatively charged Glu residues. Those mutants failed to trigger cell death in *N. benthamiana* and one of the mutants decreased its plasma membrane localization, showing the general importance of insertion of α1 helix of CNLs into plasma membrane on their immunity. Since the membrane localization of

Pit is also important for its function (Kawano et al., 2014a), it is possible that the CC domain of Pit has a funnel-shaped structure similar to that of active ZAR1 and plays an important role in its membrane localization and cell death. Our experiments showed that Pit I34E, L37E, and L41E mutants perturbed membrane localization and were localized in the cytoplasm (Figure 6). In the Pit structure model based on the active ZAR1 (PDB code 6J5T), the three hydrophobic residues (I34, L37, and L41) are located in the α2 helix but not in the α1 helix of the funnel-shaped structure, suggesting that the three hydrophobic residues are not directly involved in membrane insertion. The three hydrophobic residues, I34, L37, and L41, in the α2 helix of the Pit CC domain interact hydrophobically with V75, I78, and V79 in the α3 helix. The α3 helix is hydrophobically associated with I500 in the WHD domain and L510 in the LRR domain (Figure S4C). In addition, D77 in the α3 helix also forms a hydrogen bond with K532 in the LRR domain (Figure S4C). D77 is located at the EDVID motif in Pit (DDIVD in Pit) which is a highly conseved motif in CNLs (Bai et al., 2002). The EDVID motif directly contacts with LRR domain in the inactive ZAR1 structure (Burdett et al., 2019; Wang et al., 2019a). In the full-length MLA10 protein, the mutations of the EDVID motif in MLA10 weaken immune response but the same mutations in the CC domain fragment do not affect its autoactivity (Bai et al., 2012), suggesting that the EDVID motif is necessary for both autoinhibition and activation of MLA10. Like the ZAR1 case, it is possible that the EDVID motif serves as a signal relay from the LRR domain to the CC domain to indue the large conformational changes in the NB-LRR region. The three hydrophobic residues (I34, L37, and L41) in the α2 helix may support the funnel-shaped structure through interaction with the α3 helix, which is associated with the WHD and LRR domains. However, the substitutions of I34, L37, and L41 with Glu may destabilize this foundation for the funnel-shaped structure and consequently affect the insertion of the funnel-shaped structure formed by the N-terminal α1 helix into the membrane. Alternatively, we previously found that palmitoylation is required for plasma membrane localization of Pit (Kawano et al., 2014a) and these mutations in the CC domain of Pit may affect appropriate palmitoylation. But these speculations need to be tested in the future. The mislocalization of Pit by the mutations into the conserved

hydrophobic residues disrupted the appropriate localization of the Pit-OsSPK1 complex (Figure S5A). This may lead to the attenuation of Pit-mediated immune responses.

Author Contributions

Q. W. and Y. K. designed the study; Q. W., Y. L., K. K., J. L., D. Z., and Y. K. performed experiments and analyzed data; Q. W., K. K., and Y. K. wrote the manuscript; C. L. and D. M. gave technical support; Y. K. provided conceptual advice.

Acknowledgments

We thank the members of the Laboratory of Signal Transduction and Immunity at PSC, the Plant Immune Signal Transduction Group at Yangzhou University, and the Plant Immune Design Group at Okayama University, for invaluable support and discussions. This work was supported by the Chinese Academy of Sciences, Shanghai Institutes for Biological Sciences, Shanghai Center for Plant Stress Biology, CAS Center of Excellence for Molecular Plant Sciences, Strategic Priority Research Program of the Chinese Academy of Sciences (B) (XDB27040202), the Chinese Academy of Sciences Hundred Talents Program (173176001000162114), the National Natural Science Foundation of China (31572073, 31772246 and 3210150503), the Natural Science Foundation of Jiangsu Province (BK20190958 and BK20210796), the Natural Science Foundation of Colleges and Universities of Jiangsu Province (19KJB210001 and 21KJB210016), the CAS President's International Fellowship Initiative (2019PB0056), JSPS KAKENHI (26450055, 17K07668, and 20H02988), the Ohara Foundation, the Yakumo Foundation for Environmental Science, the Ryobi Teien Memory Foundation, and the Joint Usage/Research Center, Institute of Plant Science and Resources.

Competing financial interests

The authors declare that they have no competing financial interests.

REFERENCES

Adachi, H., Contreras, M.P., Harant, A., Wu, C.H., Derevnina, L., Sakai, T., Duggan, C., Moratto, E., Bozkurt, T.O., Maqbool, A.*, et al.* (2019). An N-terminal motif in NLR immune receptors is functionally conserved across distantly related plant species. Elife *8*.

Ade, J., DeYoung, B.J., Golstein, C., and Innes, R.W. (2007). Indirect activation of a plant nucleotide binding site-leucine-rich repeat protein by a bacterial protease. Proc Natl Acad Sci U S A *104*, 2531-2536.

Akamatsu, A., Wong, H., Fujiwara, M., Okuda, J., Nishide, K., Uno, K., Imai, K., Umemura, K., Kawasaki, T., Kawano, Y.*, et al.* (2013). An OsCEBiP/OsCERK1-OsRacGEF1-OsRac1 module is an essential component of chitin-induced rice immunity. Cell Host Microbe *13*, 465-476.

Axtell, M.J., and Staskawicz, B.J. (2003). Initiation of RPS2-specified disease resistance in Arabidopsis is coupled to the AvrRpt2-directed elimination of RIN4. Cell *112*, 369-377.

Bai, J., Pennill, L.A., Ning, J., Lee, S.W., Ramalingam, J., Webb, C.A., Zhao, B., Sun, Q., Nelson, J.C., Leach, J.E.*, et al.* (2002). Diversity in nucleotide binding site-leucine-rich repeat genes in cereals. Genome Res *12*, 1871-1884.

Bentham, A.R., Zdrzalek, R., De la Concepcion, J.C., and Banfield, M.J. (2018). Uncoiling CNLs: Structure/Function Approaches to Understanding CC Domain Function in Plant NLRs. Plant Cell Physiol *59*, 2398-2408.

Bernoux, M., Ve, T., Williams, S., Warren, C., Hatters, D., Valkov, E., Zhang, X., Ellis, J.G., Kobe, B., and Dodds, P.N. (2011). Structural and functional analysis of a plant resistance protein TIR domain reveals interfaces for self-association, signaling, and autoregulation. Cell Host Microbe *9*, 200-211.

Bigeard, J., Colcombet, J., and Hirt, H. (2015). Signaling mechanisms in pattern-triggered immunity (PTI). Mol Plant *8*, 521-539.

Bolus, S., Akhunov, E., Coaker, G., and Dubcovsky, J. (2020). Dissection of Cell Death Induction by Wheat Stem Rust Resistance Protein Sr35 and Its Matching Effector AvrSr35. Mol Plant Microbe Interact *33*, 308-319.

Burdett, H., Bentham, A.R., Williams, S.J., Dodds, P.N., Anderson, P.A., Banfield, M.J., and Kobe, B. (2019). The Plant "Resistosome": Structural Insights into Immune Signaling. Cell Host Microbe *26*, 193-201.

Casey, L.W., Lavrencic, P., Bentham, A.R., Cesari, S., Ericsson, D.J., Croll, T., Turk, D., Anderson, P.A., Mark, A.E., Dodds, P.N.*, et al.* (2016). The CC domain structure from the wheat stem rust resistance protein Sr33 challenges paradigms for dimerization in plant NLR proteins. Proc Natl Acad Sci U S A *113*, 12856-12861.

Chakraborty, J., and Ghosh, P. (2020). Advancement of research on plant NLRs evolution, biochemical activity, structural association, and engineering. Planta *252*, 101.

Chen, L., Hamada, S., Fujiwara, M., Zhu, T., Thao, N.P., Wong, H.L., Krishna, P., Ueda, T., Kaku, H., Shibuya, N.*, et al.* (2010). The Hop/Sti1-Hsp90 chaperone complex facilitates the maturation and transport of a PAMP receptor in rice innate immunity.

Cell Host Microbe *7*, 185-196.
Chen, T., Liu, D., Niu, X., Wang, J., Qian, L., Han, L., Liu, N., Zhao, J., Hong, Y., and Liu, Y. (2017). Antiviral Resistance Protein Tm-2(2) Functions on the Plasma Membrane. Plant Physiol *173*, 2399-2410.
Collier, S.M., Hamel, L.P., and Moffett, P. (2011). Cell death mediated by the N-terminal domains of a unique and highly conserved class of NB-LRR protein. Mol Plant Microbe Interact *24*, 918-931.
Cui, H., Tsuda, K., and Parker, J.E. (2015). Effector-triggered immunity: from pathogen perception to robust defense. Annu Rev Plant Biol *66*, 487-511.
Dodds, P.N., and Rathjen, J.P. (2010). Plant immunity: towards an integrated view of plant-pathogen interactions. Nat Rev Genet *11*, 539-548.
El Kasmi, F., Chung, E.H., Anderson, R.G., Li, J., Wan, L., Eitas, T.K., Gao, Z., and Dangl, J.L. (2017). Signaling from the plasma-membrane localized plant immune receptor RPM1 requires self-association of the full-length protein. Proc Natl Acad Sci U S A *114*, E7385-E7394.
Engelhardt, S., Boevink, P.C., Armstrong, M.R., Ramos, M.B., Hein, I., and Birch, P.R. (2012). Relocalization of late blight resistance protein R3a to endosomal compartments is associated with effector recognition and required for the immune response. Plant Cell *24*, 5142-5158.
Gao, Z., Chung, E.H., Eitas, T.K., and Dangl, J.L. (2011). Plant intracellular innate immune receptor Resistance to Pseudomonas syringae pv. maculicola 1 (RPM1) is activated at, and functions on, the plasma membrane. Proc Natl Acad Sci U S A *108*, 7619-7624.
Hao, W., Collier, S.M., Moffett, P., and Chai, J. (2013). Structural basis for the interaction between the potato virus X resistance protein (Rx) and its cofactor Ran GTPase-activating protein 2 (RanGAP2). J Biol Chem *288*, 35868-35876.
Hayashi, K., Yasuda, N., Fujita, Y., Koizumi, S., and Yoshida, H. (2010). Identification of the blast resistance gene Pit in rice cultivars using functional markers. Theor Appl Genet *121*, 1357-1367.
Hayashi, K., and Yoshida, H. (2009). Refunctionalization of the ancient rice blast disease resistance gene Pit by the recruitment of a retrotransposon as a promoter. Plant J *57*, 413-425.
Heidrich, K., Wirthmueller, L., Tasset, C., Pouzet, C., Deslandes, L., and Parker, J.E. (2011). Arabidopsis EDS1 connects pathogen effector recognition to cell compartment-specific immune responses. Science *334*, 1401-1404.
Hu, M., Qi, J., Bi, G., and Zhou, J.M. (2020). Bacterial Effectors Induce Oligomerization of Immune Receptor ZAR1 In Vivo. Mol Plant *13*, 793-801.
Jones, J.D., Vance, R.E., and Dangl, J.L. (2016). Intracellular innate immune surveillance devices in plants and animals. Science *354*.
Kawano, Y., Akamatsu, A., Hayashi, K., Housen, Y., Okuda, J., Yao, A., Nakashima, A., Takahashi, H., Yoshida, H., Wong, H.L.*, et al.* (2010). Activation of a Rac GTPase by the NLR family disease resistance protein Pit plays a critical role in rice innate immunity. Cell Host Microbe *7*, 362-375.
Kawano, Y., Fujiwara, T., Yao, A., Housen, Y., Hayashi, K., and Shimamoto, K. (2014a).

588 Palmitoylation-dependent membrane localization of the rice resistance protein pit
589 is critical for the activation of the small GTPase OsRac1. J Biol Chem *289*, 19079-
590 19088.
591 Kawano, Y., Kaneko-Kawano, T., and Shimamoto, K. (2014b). Rho family GTPase-
592 dependent immunity in plants and animals. Front Plant Sci *5*, 522.
593 Kawano, Y., and Shimamoto, K. (2013). Early signaling network in rice PRR- and R-
594 mediated immunity. Curr Opin Plant Biol *16*, 496–504.
595 Kim, H.S., Desveaux, D., Singer, A.U., Patel, P., Sondek, J., and Dangl, J.L. (2005).
596 The Pseudomonas syringae effector AvrRpt2 cleaves its C-terminally acylated
597 target, RIN4, from Arabidopsis membranes to block RPM1 activation. Proc Natl
598 Acad Sci U S A *102*, 6496-6501.
599 Kosami, K., Ohki, I., Nagano, M., Furuita, K., Sugiki, T., Kawano, Y., Kawasaki, T.,
600 Fujiwara, T., Nakagawa, A., Shimamoto, K.*, et al.* (2014). The crystal structure of
601 the plant small GTPase OsRac1 reveals its mode of binding to NADPH oxidase. J
602 Biol Chem *289*, 28569-28578.
603 Kourelis, J., and van der Hoorn, R.A.L. (2018). Defended to the Nines: 25 Years of
604 Resistance Gene Cloning Identifies Nine Mechanisms for R Protein Function.
605 Plant Cell *30*, 285-299.
606 Lieberherr, D., Thao, N.P., Nakashima, A., Umemura, K., Kawasaki, T., and Shimamoto,
607 K. (2005). A sphingolipid elicitor-inducible mitogen-activated protein kinase is
608 regulated by the small GTPase OsRac1 and heterotrimeric G-protein in rice. Plant
609 Physiol *138*, 1644-1652.
610 Ma, W., Wang, Y., and McDowell, J. (2018). Focus on Effector-Triggered Susceptibility.
611 Mol Plant Microbe Interact *31*, 5.
612 Macho, A.P., and Zipfel, C. (2014). Plant PRRs and the activation of innate immune
613 signaling. Mol Cell *54*, 263-272.
614 Maekawa, T., Cheng, W., Spiridon, L.N., Toller, A., Lukasik, E., Saijo, Y., Liu, P., Shen,
615 Q.H., Micluta, M.A., Somssich, I.E.*, et al.* (2011). Coiled-coil domain-dependent
616 homodimerization of intracellular barley immune receptors defines a minimal
617 functional module for triggering cell death. Cell Host Microbe *9*, 187-199.
618 Mestre, P., and Baulcombe, D.C. (2006). Elicitor-mediated oligomerization of the
619 tobacco N disease resistance protein. Plant Cell *18*, 491-501.
620 Noman, A., Aqeel, M., and Lou, Y. (2019). PRRs and NB-LRRs: From Signal
621 Perception to Activation of Plant Innate Immunity. Int J Mol Sci *20*.
622 Ono, E., Wong, H.L., Kawasaki, T., Hasegawa, M., Kodama, O., and Shimamoto, K.
623 (2001). Essential role of the small GTPase Rac in disease resistance of rice. Proc
624 Natl Acad Sci U S A *98*, 759-764.
625 Qi, D., DeYoung, B.J., and Innes, R.W. (2012). Structure-function analysis of the
626 coiled-coil and leucine-rich repeat domains of the RPS5 disease resistance protein.
627 Plant Physiol *158*, 1819-1832.
628 Rairdan, G.J., Collier, S.M., Sacco, M.A., Baldwin, T.T., Boettrich, T., and Moffett, P.
629 (2008). The coiled-coil and nucleotide binding domains of the Potato Rx disease
630 resistance protein function in pathogen recognition and signaling. Plant Cell *20*,
631 739-751.

Shen, Q.H., Saijo, Y., Mauch, S., Biskup, C., Bieri, S., Keller, B., Seki, H., Ulker, B., Somssich, I.E., and Schulze-Lefert, P. (2007). Nuclear activity of MLA immune receptors links isolate-specific and basal disease-resistance responses. Science *315*, 1098-1103.

Slootweg, E., Roosien, J., Spiridon, L.N., Petrescu, A.J., Tameling, W., Joosten, M., Pomp, R., van Schaik, C., Dees, R., Borst, J.W., *et al.* (2010). Nucleocytoplasmic distribution is required for activation of resistance by the potato NB-LRR receptor Rx1 and is balanced by its functional domains. Plant Cell *22*, 4195-4215.

Swiderski, M.R., Birker, D., and Jones, J.D. (2009). The TIR domain of TIR-NB-LRR resistance proteins is a signaling domain involved in cell death induction. Mol Plant Microbe Interact *22*, 157-165.

Takken, F.L., Albrecht, M., and Tameling, W.I. (2006). Resistance proteins: molecular switches of plant defence. Curr Opin Plant Biol *9*, 383-390.

Tameling, W.I., Nooijen, C., Ludwig, N., Boter, M., Slootweg, E., Goverse, A., Shirasu, K., and Joosten, M.H. (2010). RanGAP2 mediates nucleocytoplasmic partitioning of the NB-LRR immune receptor Rx in the Solanaceae, thereby dictating Rx function. Plant Cell *22*, 4176-4194.

Tanaka, K., Caaveiro, J.M., Morante, K., Gonzalez-Manas, J.M., and Tsumoto, K. (2015). Structural basis for self-assembly of a cytolytic pore lined by protein and lipid. Nat Commun *6*, 6337.

Wang, G.F., Ji, J., El-Kasmi, F., Dangl, J.L., Johal, G., and Balint-Kurti, P.J. (2015). Molecular and functional analyses of a maize autoactive NB-LRR protein identify precise structural requirements for activity. PLoS Pathog *11*, e1004674.

Wang, J., Han, M., and Liu, Y. (2021). Diversity, structure and function of the coiled-coil domains of plant NLR immune receptors. J Integr Plant Biol *63*, 283-296.

Wang, J., Hu, M., Wang, J., Qi, J., Han, Z., Wang, G., Qi, Y., Wang, H.W., Zhou, J.M., and Chai, J. (2019a). Reconstitution and structure of a plant NLR resistosome conferring immunity. Science *364*.

Wang, J., Wang, J., Hu, M., Wu, S., Qi, J., Wang, G., Han, Z., Qi, Y., Gao, N., Wang, H.W., *et al.* (2019b). Ligand-triggered allosteric ADP release primes a plant NLR complex. Science *364*, 43.

Wang, Q., Li, Y., Ishikawa, K., Kosami, K.I., Uno, K., Nagawa, S., Tan, L., Du, J., Shimamoto, K., and Kawano, Y. (2018). Resistance protein Pit interacts with the GEF OsSPK1 to activate OsRac1 and trigger rice immunity. Proc Natl Acad Sci U S A *115*, E11551-E11560.

Williams, S.J., Sohn, K.H., Wan, L., Bernoux, M., Sarris, P.F., Segonzac, C., Ve, T., Ma, Y., Saucet, S.B., Ericsson, D.J., *et al.* (2014). Structural basis for assembly and function of a heterodimeric plant immune receptor. Science *344*, 299-303.

Wong, H.L., Akamatsu, A., Wang, Q., Higuchi, M., Matsuda, T., Okuda, J., Kosami, K.I., Inada, N., Kawasaki, T., Kaneko-Kawano, T., *et al.* (2018). In vivo monitoring of plant small GTPase activation using a Forster resonance energy transfer biosensor. Plant Methods *14*, 56.

Wroblewski, T., Spiridon, L., Martin, E.C., Petrescu, A.J., Cavanaugh, K., Truco, M.J., Xu, H., Gozdowski, D., Pawlowski, K., Michelmore, R.W., *et al.* (2018). Genome-

676 wide functional analyses of plant coiled-coil NLR-type pathogen receptors reveal
677 essential roles of their N-terminal domain in oligomerization, networking, and
678 immunity. PLoS Biol *16*, e2005821.
679 Yalovsky, S. (2015). Protein lipid modifications and the regulation of ROP GTPase
680 function. J Exp Bot *66*, 1617-1624.
681 Zhou, J.M., and Zhang, Y. (2020). Plant Immunity: Danger Perception and Signaling.
682 Cell *181*, 978-989.
683 Zhou, Z., Pang, Z., Zhao, S., Zhang, L., Lv, Q., Yin, D., Li, D., Liu, X., Zhao, X., Li,
684 X.*, et al.* (2019). Importance of OsRac1 and RAI1 in signalling of NLR protein-
685 mediated resistance to rice blast disease. New Phytol.
686 Zou, S., Wang, H., Li, Y., Kong, Z., and Tang, D. (2018). The NB-LRR gene Pm60
687 confers powdery mildew resistance in wheat. New Phytol *218*, 298-309.
688
689

690 **FIGURE LEGENDS**

691 **Figure 1. The CC domain and full-length Pit self-associate**

692 **A**, Co-IP assay to assess self-association of full-length Pit in *N. benthamiana*. Total
693 protein extract was immunoprecipitated with anti-HA antibody, and western blotting
694 was then carried out with anti-HA and anti-Myc antibodies. **B**, Yeast two-hybrid assay
695 to test self-association of the Pit CC domain. Growth of yeast cells coexpressing GAL4-
696 AD or GAL4-BD fused with the CC domain of Pit on selective medium without
697 histidine (-His) represents a positive interaction. AD: GAL4 activation domain, BD:
698 GAL4 DNA-binding domain. **C**, Co-IP assay to assess self-association of the Pit CC
699 domain in *N. benthamiana*. Total protein extract was immunoprecipitated with anti-
700 GFP antibody, and western blotting was then carried out with anti-GFP and anti-Myc
701 antibodies. These bands are from same blot. **D**, GST pull-down assay to verify the self-
702 association of the Pit CC domain. Purified GST or GST-tagged Pit CC immobilized on
703 Sepharose was incubated with His-SUMO-tagged Pit CC. After washing, the bound
704 proteins were eluted by addition of SDS loading buffer for immunoblotting with anti-
705 GST and anti-SUMO.

706

707 **Figure 2. Conserved hydrophobic residues in the Pit CC domain are not involved**
708 **in Pit self-association**

709 **A**, Multiple alignment of Pit with various CNLs. **B**, Structure model of the Pit CC
710 domain, based on the MLA10 CC domain (Protein Data Bank ID code 3QFL), shows
711 the elongated dimer (blue and pink), stabilized by hydrophobic residues (I34, L37, and
712 L41). The figure was drawn using PyMOL. **C**, *In vitro* pull-down assay to test the self-
713 association of Pit CC mutants. Purified GST or GST-tagged Pit CC mutants
714 immobilized on Sepharose was incubated with His-SUMO-tagged Pit CC mutants.
715 After washing, the bound proteins were eluted by addition of SDS loading buffer for
716 immunoblotting. Anti-GST and anti-SUMO antibodies were used for western blotting.
717 **D**, Yeast two-hybrid assay to test self-association of Pit CC mutants. Growth of yeast
718 cells coexpressing GAL4-AD or GAL4-BD fused with the CC domain of Pit on
719 selective medium (-LWHA) represents a positive interaction. 10^{-1}, 10^{-2}, and 10^{-3}

indicate dilution ratio. **E**, Co-IP assay to examine self-association of full-length Pit mutants in *N. benthamiana*. Total protein extract was immunoprecipitated with anti-GFP antibody, and western blottingwas then carried out with anti-GFP and anti-Myc antibodies. The post-transfer membrane was stained with Ponceau S. These bands are from same blot.

Figure 3. Conserved hydrophobic residues in the Pit CC domain contribute to Pit-mediated immune signaling

A, Cell death phenotypes induced by transient expression of Pit mutants in *N. benthamiana*. Photos were taken at 2 dpi. The circles indicate the infiltrated regions. **B**, Effect of three hydrophobic residues on Pit D485V-induced ROS production in *N. benthamiana*. ROS production was examined by DAB staining at 2 dpi. **C**, Cell death activity of Pit mutants in rice protoplasts. Relative luciferase activity (GUS=100) is shown. Data are expressed as mean ± standard error (SE) (**$P < 0.01$, $n = 3$). **D** and **E**, Responses, in plants overexpressing Pit WT or mutants, to infection with the incompatible *M. oryzae* race 007.0. **D**, Photograph shows typical phenotypes of transgenic and WT plants at 7 dpi. Five independent lines were tested for each mutants. **E**, Statistical analysis of lesion length was performed at 6 dpi. Relative lesion length [Nippobnare (NB) = 1] is shown. Data are expressed as mean ± standard error (SE) (*$P < 0.05$; $n \geq 30$). **F**, Growth of the incompatible *M. oryzae* race in Nipponbare wild-type plants and transgenic plants overexpressing Pit WT or mutants. Relative infection ratio (NB = 1) is shown. Data are expressed as mean ± standard error (SE) (*$P < 0.05$; **$P < 0.01$; $n = 10$).

Figure 4. Mutations in three hydrophobic residues do not affect binding to OsSPK1 or OsRac1 but perturb Pit-mediated OsRac1 activation

A, Co-IP to test the interaction between OsSPK1 and Pit hydrophobic residue mutants in *N. benthamiana*. Total protein extract was immunoprecipitated with anti-GFP antibody, and western blotting was then carried out with anti-GFP and anti-HA antibodies. The post-transfer membrane was stained with Ponceau S. **B**, Co-IP to test

the interaction between OsRac1 and Pit hydrophobic residue mutants in *N. benthamiana*. Total protein extract was immunoprecipitated with anti-GFP antibody, and western blotting was then carried out with anti-GFP and anti-Myc antibodies. The post-transfer membrane was stained with Ponceau S. **C** and **D**, *In vivo* OsRac1 activation by Pit hydrophobic residues mutants. **C**, Emission ratio images of confocal laser-scanning micrographs of rice protoplasts coexpressing Raichu-OsRac1 and the indicated Pit mutants, or negative control GUS. Scale bars, 5 μm. **D**, Quantification of normalized emission ratios of Venus to CFP. Data are expressed as mean ± standard error (SE) (**$P < 0.01$, $n = 60$).

Figure 5. The CC domain of various NLRs

A, The main chains of the CC domain structure of Sr33 (blue, solution NMR condition, Protein Data Bank ID code 2NCG), Rx (light blue, crystal condition, Protein Data Bank ID code 4M70), and inactivated ZAR1 (orange, electron microscopy condition, 6J5W, residues 1–113) were superimposed using PyMOL. **B,** Comparison of conserved hydrophobic residues of Pit (residues 1–115), inactivated ZAR1 (residues 1–113), Sr33, and Rx. The side chains of three key hydrophobic residues in Pit (I34, L37, and L41) and equivalent residues in inactivated ZAR1 1–113 (L31, L34, and L38), Rx (I33, L36, and L40), Sr33 (L24, F27, and L31), as well as the side chains of amino acids thought to be involved in hydrophobic interactions with these three residues, are shown in stick representation. **C,** Structure model and domain composition of full-length Pit, based on inactivated ZAR1 (Protein Data Bank ID code 6J5W), shows the monomeric state. The figure was drawn using PyMOL.

Figure 6. Mutations in the conserved hydrophobic residues of Pit influence its plasma membrane localization

A and **B**, Subcellular localization of Pit mutants in rice protoplasts and *N. benthamiana* leaves. **A**, Rice protoplasts were cotransfected with the indicated *Pit-Venus* mutants and *OsFLS2-mCherry.* Scale bars, 5 μm. **B**, Tobacco leaves were injected

780 with *Agrobacterium* carrying *Pit-GFP* mutants (green) and stained with FM4-64 (red:
781 plasma membrane marker). Enlarged images of the boxed areas are shown in the right
782 panels. Scale bars, 25 μm. **C**, Distribution of Pit-Myc mutants in tobacco leaves.
783 Immunoblotting was performed with anti-Myc (for Pit mutants), anti-H^+ATPase (PM
784 marker), and anti-cAPX (cytoplasm marker) antibodies. T: total extract, S: soluble
785 fraction, M: microsomal fraction. M (3×) indicates three times enrichment relative to T
786 or S. Ponceau staining used as the loading control. These bands are from the same blot.
787
788
789

EXPERIMENTAL PROCEDURES

Plasmid Construction

For Gateway system-constructed plasmids, the target genes and fragments were first cloned into the pENTR/D-TOPO vector (Invitrogen), and then transferred by LR reaction into multiple destination vectors (including pGWB series, p2K-GW, pVP16-NLS-VP16-GW, pBTM116-LexA) depending on the experimental requirements. For site-directed mutagenesis, overlapping PCR amplification using site-specific and mutagenic primers and pENTR templates was employed to generate *Pit* mutants. For pull-down and yeast two-hybrid assays, *Pit* mutants were directly cloned into the pSUMO-6×His-SUMO, pGADT7-AD, and pGBKT7-BD vectors, using restriction enzymes and T4 ligase (New England Biolabs).

Yeast Two-Hybrid Assay

The Y2HGold-GAL4 system was used to test interactions between target proteins by transforming GAL4-AD/BD fused *Pit* plasmids into Y2HGold chemically competent cells (Weidibio: YC1002).

Transient Expression and HR Assays

Agroinfiltration of *N. benthamiana* was conducted as described previously (Kawano et al., 2010). *Agrobacterium tumefaciens* strain GV3101 pMP90 carrying the helper plasmid pSoup and binary plasmids was grown overnight at 28°C to an optical density at 600 nm (OD_{600}) of around 0.8. Agrobacterial cells were harvested, resuspended in 10 mM $MgCl_2$, 10 mM MES-NaOH (pH 5.6), and 150 μM acetosyringone, adjusted to OD_{600} = 0.4, and incubated at 23°C for 2-3 h before infiltration. We also used the p19 silencing suppressor to enhance gene expression. For coexpression of two proteins, *Agrobacterium* carrying the appropriate two constructs and p19 helper plasmid-containing bacteria were mixed at 1:1:1 volume ratio. The uppermost 3 or 4 leaves of 4-week-old *N. benthamiana* plants were selected for injection, and inoculated plants were kept in a growth room at 25°C for 2 days.

Transient expression of Pit mutants in tobacco leaves was performed according to the

method described above. Each bacterial inoculum was infiltrated in a circle with a diameter of 1 cm on each of 15 leaves for three independent experiments. After 2-3 days, cell death symptoms became visible and were photographed.

For ROS detection and quantification assay, the infiltrated leaves expressing Pit mutants or negative control GFP were collected and floated in 1 mg/ml DAB solution for 5 h at room temperature. To visualize ROS *in situ*, the leaves were then decolorized with ethanol by boiling several times in a microwave oven until the chlorophyll was removed completely. ROS production of each sample was quantified by measuring the pixel intensities of the infected regions using ImageJ software (National Institutes of Health). The mean pixel intensity from three spots outside the infiltrated regions on each leaf was used to subtract background. Relative DAB staining intensity was calculated based on the mean pixel intensity of the GFP-infected region on each leaf to compare between different leaves.

Plant Growth and Infection

All of transgenic rice plants used in this study were produced by the core facility of Shanghai Center for Plant Stress Biology. T0 generation of transgenic plants were used for infection analysis because introduced *Pit* WT gene did not sucessfully transmit T1 generation due to unknown reasons. Nipponbare plants were grown at 30°C for 5-6 weeks before being infected with the *M. oryzae* strain Ina86-137 (Race 007.0) (Hayashi and Yoshida, 2009). Infection of leaf blades by the punch method was performed as reported previously (Kawano et al., 2010; Ono et al., 2001). Lesion length and fungus growth were measured at 7 dpi. Photographs of disease lesions were taken at 6 dpi.

Expression Analysis

Total RNA from rice was extracted using TRIzol reagent (Invitrogen). Total RNA (500 ng) was used for cDNA synthesis with a commercial kit (Vazyme) according to the manufacturer's protocol. The cDNA was analyzed semi-quantitatively using normal polymerase mix. Total genomic DNA was extracted by the CTAB method and then subjected to quantitative analysis using SYBR Green Supermix (Bio-Rad) on a CFX96

Touch Real-Time PCR Detection System (Bio-Rad). *OsUbiquitin* was used as an internal control for normalization. Sequences of RT-PCR and RT-qPCR primers are listed in supplementary Table 1.

Raichu-OsRac1 FRET Analysis

The Raichu intramolecular FRET system was applied as described previously (Kawano et al., 2010; Wong et al., 2018). Rice protoplasts were transformed with *Raichu-OsRac1* and *Pit* mutants or *GUS* vectors by the PEG method. Images of transformed cells were captured using a LEICA SMD FLCS microscope. Raichu-OsRac1 was excited using a 440 nm solid-state laser. The Venus and CFP filters were 550 ± 25 nm and 470 ± 20 nm, respectively.

Protein Expression and Purification

His-SUMO tag- and glutathione-S-transferase (GST) tag-fused Pit CC (amino acids 1-140) were expressed in *Escherichia coli* strain BL21(DE3) Codon Plus. The bacteria were cultured at 37°C until the OD_{600} of the suspension of the medium was around 0.8. The recombinant proteins were induced with 0.3 mM IPTG for 12 h at 18°C. For protein purification, the bacterial cells were collected, resuspended, and sonicated in a lysis buffer (20 mM Tris-HCl [pH 8.0], 150 mM NaCl, 1 mM DTT). The proteins were then purified by affinity chromatography using Ni-NTA agarose resin and Glutathione Sepharose 4B resin (GE Healthcare), respectively.

***In Vitro* Pull-down Assay**

Equal amounts of His-SUMO-Pit CC and GST-Pit CC WT or mutated proteins in binding buffer (50 mM Tris-HCl [pH 7.5], 150 mM NaCl, 0.1% Triton X-100, 1 mM EDTA, and 1 mM DTT) were mixed to 200 µl for each reaction and incubated at 4°C for 5 min with gentle rotation. Glutathione Sepharose 4B resin was added to the solution for precipitation. The beads were washed five times with binding buffer and separated from the solution by centrifugation at 2500 × *g* for 2 min. The proteins were then eluted with 100 µl 2×SDS loading buffer for immunoblotting. Anti-SUMO (GenScript:

A01693) and anti-GST (Abmart: M20007) antibodies were used.

Subcellular Localization

Confocal fluorescence pictures were recorded under a Leica TCS-SP8 microscope, using 60×water-immersion objectives. A 488-nm laser was used to image GFP; a 514-nm laser was used to image Venus; and a 598-nm laser was used to image mCherry. For samples stained with a plasma membrane marker, FM4-64 (Invitrogen: F34653) solution was injected to the infiltrated leaves before harvesting and observation. The signals of FM4-64 were excited with a 566-nm laser.

Luciferase Activity Assay in Rice Protoplasts

Isolation of rice protoplasts and PEG transformation were performed as described previously (Kawano et al., 2010; Wang et al., 2018). Protein preparation and luciferase–substrate interaction were conducted with a Luciferase Assay Report Kit (Promega). Luciferase activity was measured by a microplate reader (Thermo Scientific Varioskan Flash). We used mean values of three independent replications.

Co-immunoprecipitation Assays

An *in vivo* co-immunoprecipitation (co-IP) assay was performed as previously reported (Wang et al., 2018). The infiltrated tobacco leaves were ground to powder in liquid nitrogen and homogenized in IP buffer (50 mM Tris-HCl [pH 7.5], 150 mM NaCl, 10% glycerol, 0.2% NP-40, 1 mM EDTA, 5 mM DTT, and EDTA-free protease inhibitor [Roche]). Anti-GFP agarose resin (Chromotek, GFP-Trap A, gta-20) was added to the extracted protein solution for precipitation. The GFP beads were washed five times and then subjected to immunoblot analysis together with input samples. Anti-Myc (Cell Signaling: #2276S), anti-HA (Roche: 11867423001), and anti-GFP (Abcam: ab6556) antibodies were used for western blot.

Bimolecular Fluorescence Complementation (BiFC)

OsSPK1-cYFP, cYFP-OsRac1, and Pit-nYFP mutants were transiently expressed in *N.*

benthamiana leaves according to the method described above. The signals of YFP were observed under a Leica TCS-SP8 microscope. A 514-nm laser was used to excite the YFP fluorescence and signals between 525 nm and 575 nm were recorded.

Cell fractionation

Liquid nitrogen-frozen tobacco leaves were ground to fine powder with a pestle and mortar, and protein extracts expressing were separated into membrane and soluble protein fractions, as described previously (El Kasmi et al., 2017). Anti-cAPX (AS06 180: cytosol; Agrisera) and anti-H^+ATPase (AS07 260: plasma membrane; Agrisera) antibodies were used.

Statistical Analysis and Biological Repetitions

Means were compared by using a *t* test (two-tailed; type 2). SEs were calculated in Microsoft Excel software. All of assays (including Co-IP, Y2H, Pull down, etc.) in this study were independently repeated at least three times.

Accession number

Pit: AB379815.1; *OsRac1*: AB029508.1; *OsSPK1*: XM_015775852.2.

Supplementary information includes the following items:

1. Five supplementary figures and legends.

Figure S1 is related to Figure 1.

Figure S2 is related to Figures 2 and 3.

Figure S3 is related to Figures 3 and 4.

Figure S4 is related to Figure 5.

Figure S5 is related to Figure 6.

2. One supplementary table

Table S1. List of primers for experimental procedures

Figure S1. The CC domain of Pit is not sufficient to induce cell death

A, Cell death phenotypes induced by transient expression of Pit N-terminal deletion mutants in *N. benthamiana*. Photos were taken at 2 dpi. The circles indicate the infiltrated regions. Numbers indicate amino acid boundaries of Pit mutants. **B**, Myc-tagged Pit mutants were transiently expressed in *N. benthamiana* leaves. After 2 days, the total proteins of infiltrated leaves were extracted for immunoblotting with anti-Myc antibody. NI indicates non-infiltrated leaves. The post-transfer membrane was stained with Ponceau S and used as an internal control. **C**, protein sequence alignment among the CC domain of R proteins. Each background color indicates minimal region of NLRs required for cell death induction or oligomerization.

Figure S2. Effect of conserved hydrophobic residue mutations on Pit signaling

A, Protein expression of Pit CC WT and mutants in Y2HGold yeast cells. Anti-HA and anti-Myc antibodies were used for western blot to detect baits and preys, respectively. The post-transfer membrane was stained with Ponceau S. **B**, Quantitative analysis of the effect of I34, L37, and L41 mutation on Pit D485V-induced ROS production in *N. benthamiana*. Bars indicate DAB staining intensity relative to that observed after infiltration with negative control GFP. Data are expressed as mean ± standard error (SE) (**: $P < 0.01$; $n = 10$). Relative intensity of DAB staining (GUS=50) is shown. **C**, HA-tagged Pit mutants were transiently expressed in *N. benthamiana* leaves. After 2 days, the total proteins of infiltrated leaves were extracted for immunoblotting with anti-HA antibody. NI indicates non-infiltrated leaves. The post-transfer membrane was stained with Ponceau S and used as an internal control. **D**, Venus-tagged Pit mutants were transiently expressed in rice protoplasts. After 14 h, total protein was extracted with SDS loading buffer, and western blotting was then carried out with anti-GFP antibody. NT indicates a non-transformed sample. The post-transfer membrane was stained with Ponceau S.

Figure S3. Three hydrophobic residues in the Pit CC domain are not necessary for binding to OsSPK1

A, Transcript levels of exogenous *Pit* WT and *Pit* mutants were measured by RT-PCR. Numbers indicate independent transgenic lines. *Ubiquitin* was used as an internal control. **B**, *In vitro* binding assay between Pit CC mutants and OsSPK1. Purified GST or GST-tagged Pit CC mutants immobilized on Sepharose were incubated with His-SUMO-tagged OsSPK1 (amino acids 1334-1835). After washing, the bound proteins were eluted by addition of SDS loading buffer. Anti-GST and anti-SUMO antibodies were used for subsequent western blotting analysis. **C**, Co-IP to analyze the interaction in *N. benthamiana* between OsSPK1 (amino acids 1002-1835) and full-length Pit with mutations in three conserved hydrophobic residues. Total protein extract was immunoprecipitated with anti-GFP antibody, and western blotting was then carried out with anti-GFP and anti-Myc antibodies. The post-transfer membrane was stained with Ponceau S.

Figure S4. Homology modeling of Pit using activated ZAR1 as a template

A, Comparison of the Pit structure models based on the active and inactive ZAR1. The structure models of Pit are based on the structures of inactivated ZAR1 (Protein Data Bank ID code 6J5W) and activated ZAR1 (Protein Data Bank ID code 6J5T). Conformational changes (black arrows) between the Pit structure models based on the active and inactive ZAR1 occur around the hinge linking the HD domain (blue) and WHD domain (pink) of Pit and also at the α1 helix of the CC domain (orange). **B,** Structure model of the Pit pentamer based on the activated ZAR1. The extreme N-terminal α1 helix of the Pit pentamer may be required for the plasma membrane association of Pit. The CC, NBD, HD1, WHD, and LRR domains are shown in orange, green, blue, pink, and yellow, respectively. **C,** Hydrophobic interactions among α2 (I34, L37, and L41), α3 (F73, V75, I78, and V79), and WHD domain (I500 and L510) in the Pit pentamer structure model based on the activated ZAR1 are shown. Residues that may be important for hydrophobic interactions in Pit function are shown in green, and hydrogen-bonded side chains are shown in light blue. **D,** Comparison of the interaction around α1 of the activated ZAR1 structure (Protein Data Bank ID code 6J5T) and the Pit oligomer structure model based on the active ZAR1. Residues involved in

hydrophobic interaction around α1 are shown in green, and hydrogen-bonded side chains are shown in light blue. The figure was drawn using PyMOL.

Figure S5. Subcellular-interaction locations between Pit mutants and OsSPK1 or OsRac1

A and **B**, BiFC to detect interactions between Pit hydrophobic residue mutants and OsSPK1 (**A**) or OsRac1 (**B**). Expression constructs were transiently expressed in *N. benthamiana* after agroinfiltration. Empty vector served as a negative control. FM4-64 was used as a plasma membrane marker. Images were captured at 45 h post-infiltration. Enlarged images of the boxed areas in (A and B) are shown in the right panels. Scale bars, 25 μm.

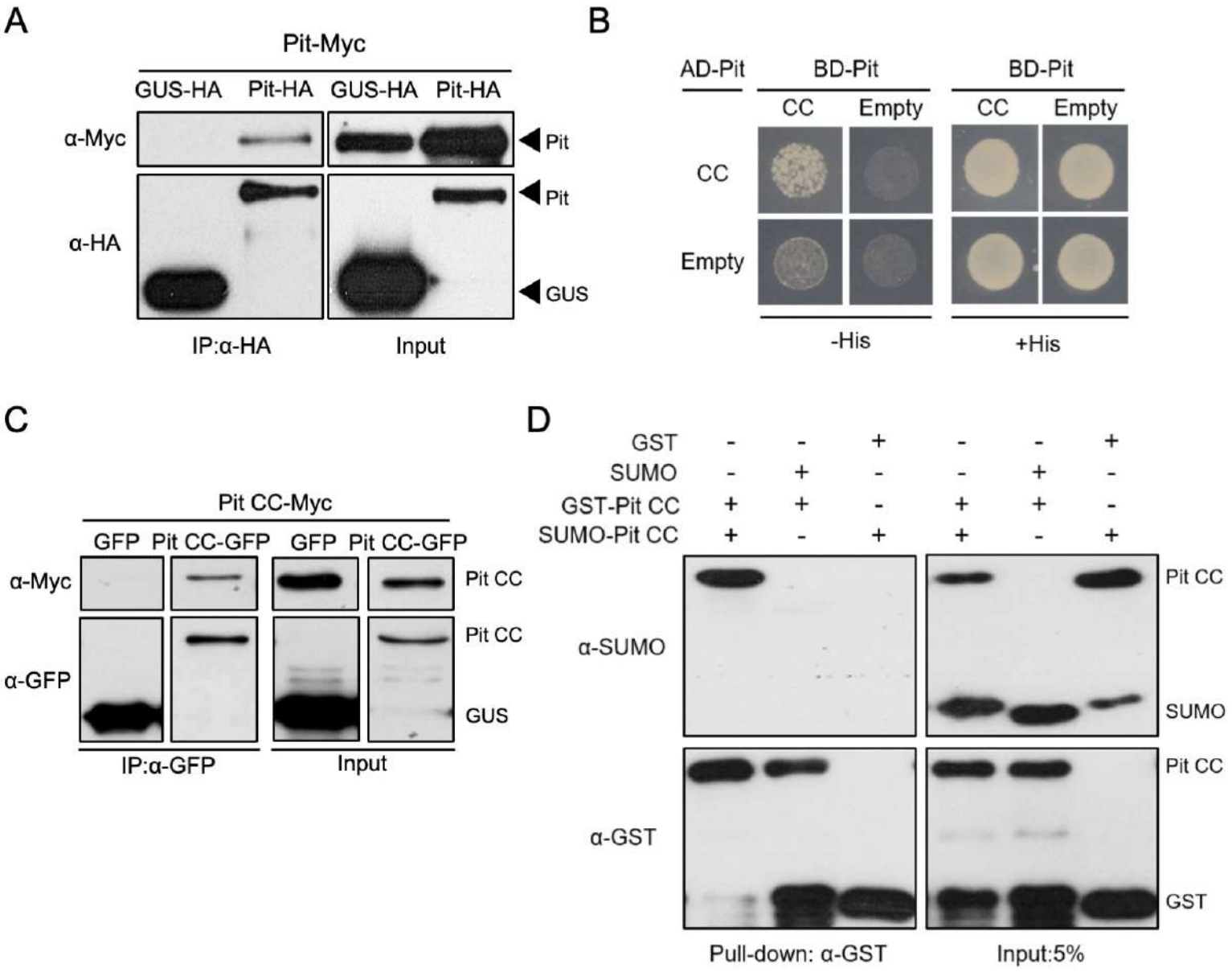

Figure 1. The CC domain and full-length Pit self-associate

A, Co-IP assay to assess self-association of full-length Pit in *N. benthamiana*. Total protein extract was immunoprecipitated with anti-HA antibody, and western blotting was then carried out with anti-HA and anti-Myc antibodies. **B**, Yeast two-hybrid assay to test self-association of the Pit CC domain. Growth of yeast cells coexpressing GAL4-AD or GAL4-BD fused with the CC domain of Pit on selective medium without histidine (-His) represents a positive interaction. AD: GAL4 activation domain, BD: GAL4 DNA-binding domain. **C**, Co-IP assay to assess self-association of the Pit CC domain in *N. benthamiana*. Total protein extract was immunoprecipitated with anti-GFP antibody, and western blotting was then carried out with anti-GFP and anti-Myc antibodies. These bands are from same blot. **D**, GST pull-down assay to verify the self-association of the Pit CC domain. Purified GST or GST-tagged Pit CC immobilized on Sepharose was incubated with His-SUMO-tagged Pit CC. After washing, the bound proteins were eluted by addition of SDS loading buffer for immunoblotting with anti-GST and anti-SUMO.

Wang et al., Figure 2

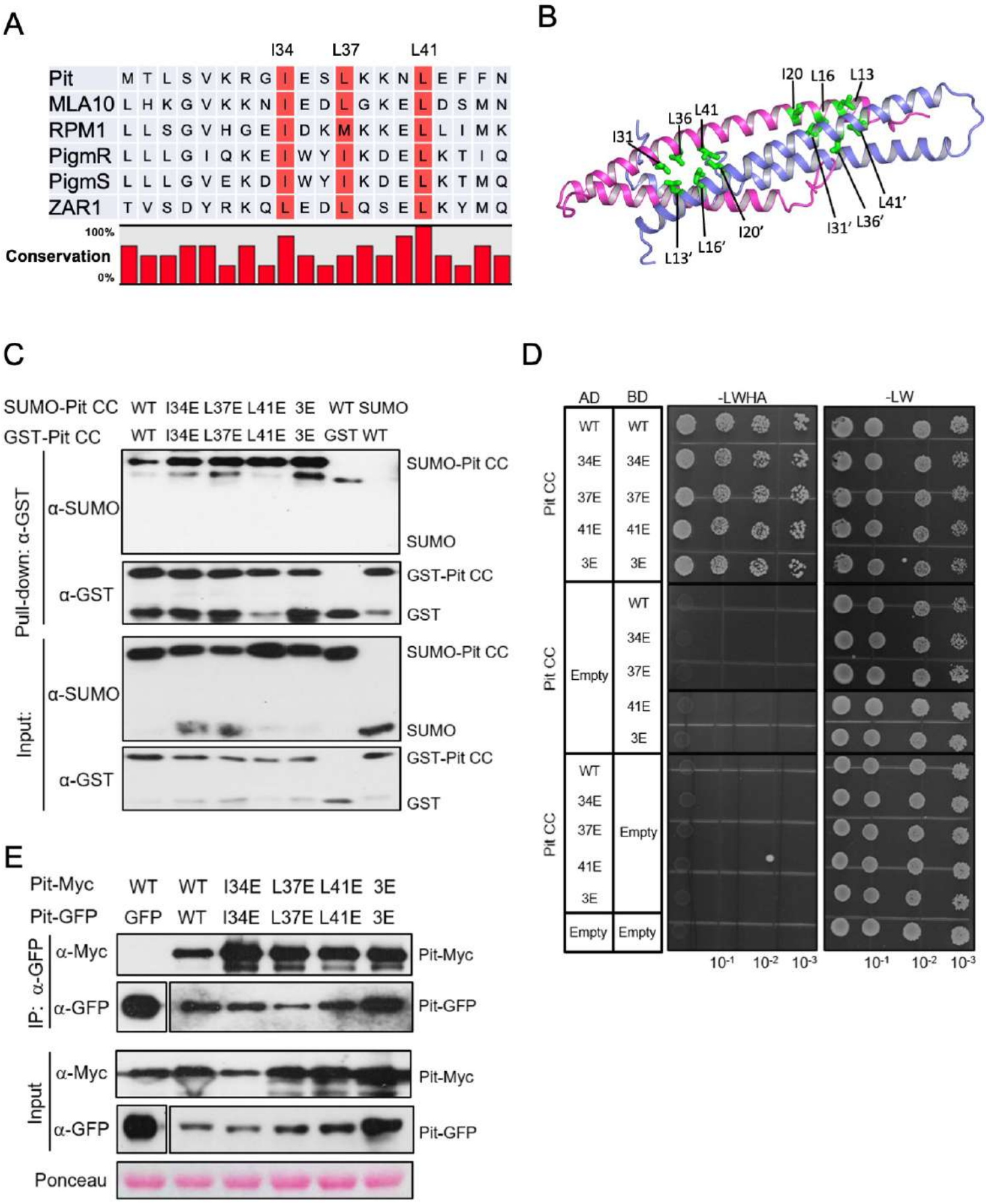

Figure 2. Conserved hydrophobic residues in the Pit CC domain are not involved in Pit self-association

A, Multiple alignment of Pit with various CNLs. **B**, Model structure of the Pit CC domain, based on the MLA10 CC domain (Protein Data Bank ID code 3QFL), shows the elongated dimer (blue and pink), stabilized by hydrophobic residues (I34, L37, and L41). The figure was drawn using PyMOL. **C**, *In vitro* pull-down assay to test the self-association of Pit CC mutants. Purified GST or GST-tagged Pit CC mutants immobilized on Sepharose was incubated with His-SUMO-tagged Pit CC mutants. After washing, the bound proteins were eluted by addition of SDS loading buffer for immunoblotting. Anti-GST and anti-SUMO antibodies were used for western blotting. **D**, Yeast two-hybrid assay to test self-association of Pit CC mutants. Growth of yeast cells coexpressing GAL4-AD or GAL4-BD fused with the CC domain of Pit on selective medium (-LWHA) represents a positive interaction. 10^{-1}, 10^{-2}, and 10^{-3} indicate dilution ratio. **E**, Co-IP assay to examine self-association of full-length Pit mutants in *N. benthamiana*. Total protein extract was immunoprecipitated with anti-GFP antibody, and western blottingwas then carried out with anti-GFP and anti-Myc antibodies. The post-transfer membrane was stained with Ponceau S. These bands are from same blot.

Wang et al., Figure 3

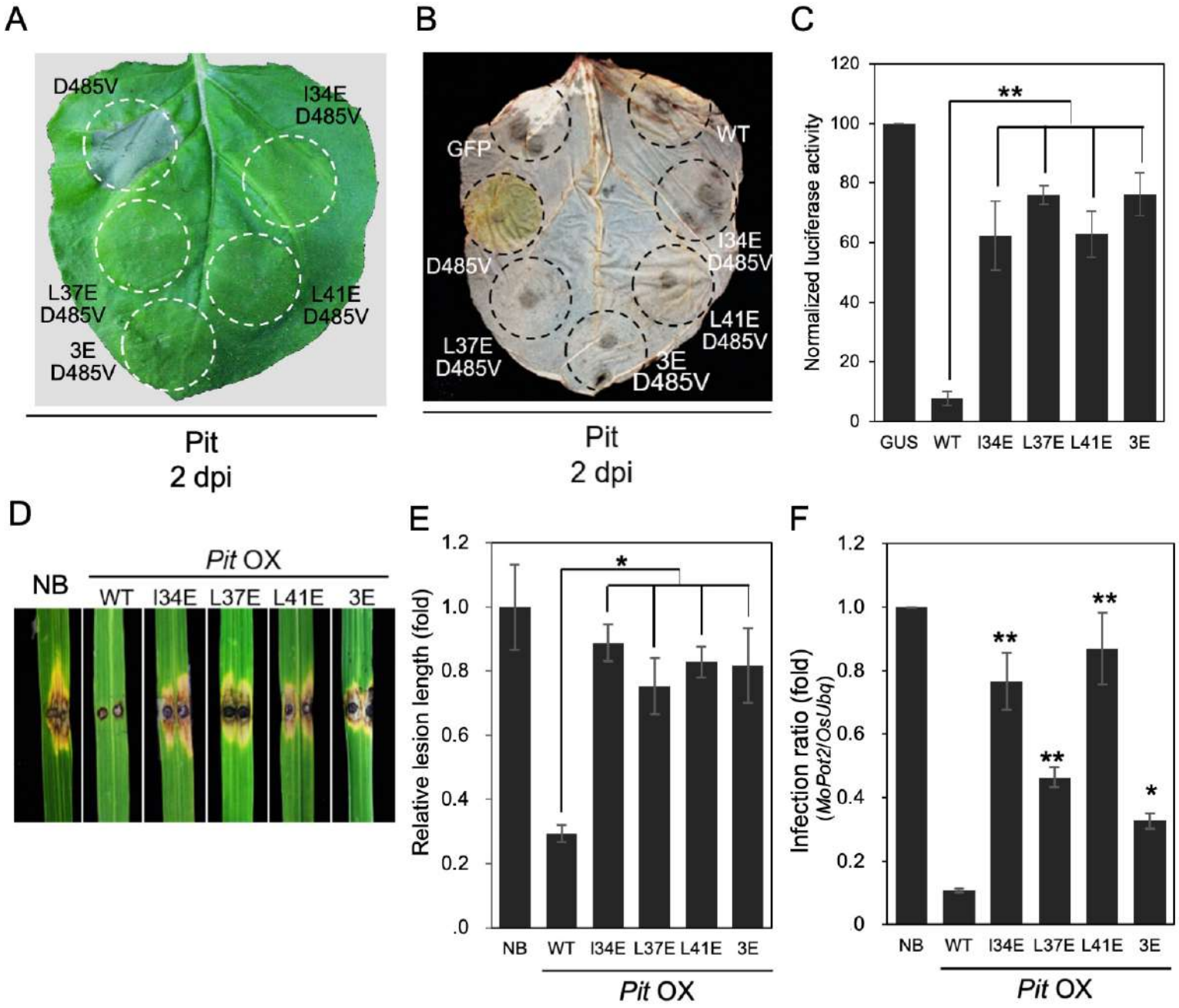

Figure 3. Conserved hydrophobic residues in the Pit CC domain contribute to Pit-mediated immune signaling
A, Cell death phenotypes induced by transient expression of Pit mutants in *N. benthamiana*. Photos were taken at 2 dpi. The circles indicate the infiltrated regions. **B**, Effect of three hydrophobic residues on Pit D485V-induced ROS production in *N. benthamiana*. ROS production was examined by DAB staining at 2 dpi. **C**, Cell death activity of Pit mutants in rice protoplasts. Relative luciferase activity (GUS=100) is shown. Data are expressed as mean ± standard error (SE) (**$P < 0.01$, $n = 3$). **D** and **E**, Responses, in plants overexpressing Pit WT or mutants, to infection with the incompatible *M. oryzae* race 007.0. **D**, Photograph shows typical phenotypes of transgenic and WT plants at 7 dpi. Five independent lines were tested for each mutants. **E**, Statistical analysis of lesion length was performed at 6 dpi. Relative lesion length [Nippobnare (NB) = 1] is shown. Data are expressed as mean ± standard error (SE) (*$P < 0.05$; $n \geq 30$). **F**, Growth of the incompatible *M. oryzae* race in Nipponbare wild-type plants and transgenic plants overexpressing Pit WT or mutants. Relative infection ratio (NB = 1) is shown. Data are expressed as mean ± standard error (SE) (*$P < 0.05$; **$P < 0.01$; $n = 10$).

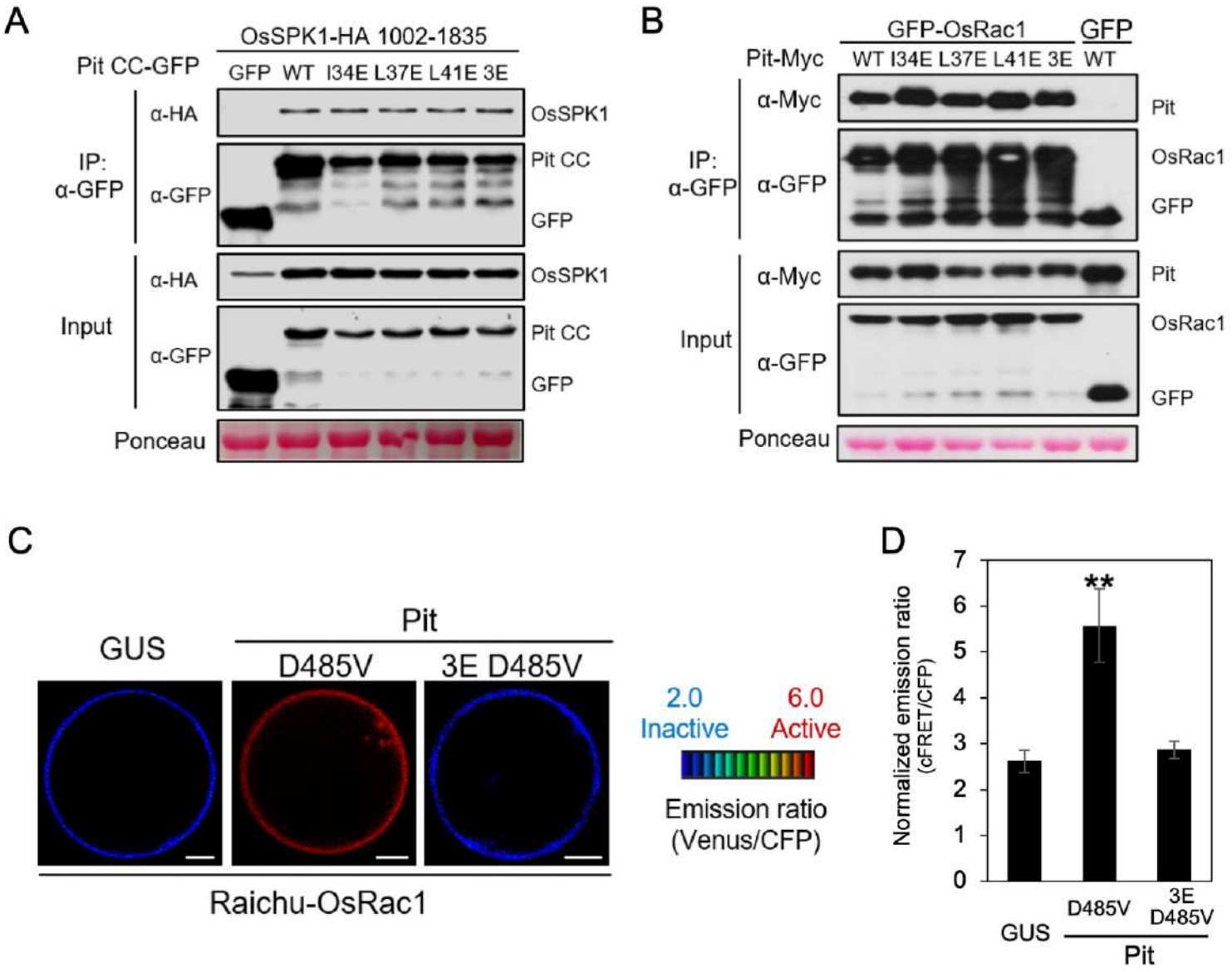

Figure 4. Mutations in three hydrophobic residues do not affect binding to OsSPK1 or OsRac1 but perturb Pit-mediated OsRac1 activation

A, Co-IP to test the interaction between OsSPK1 and Pit hydrophobic residue mutants in *N. benthamiana*. Total protein extract was immunoprecipitated with anti-GFP antibody, and western blotting was then carried out with anti-GFP and anti-HA antibodies. The post-transfer membrane was stained with Ponceau S. **B**, Co-IP to test the interaction between OsRac1 and Pit hydrophobic residue mutants in *N. benthamiana*. Total protein extract was immunoprecipitated with anti-GFP antibody, and western blotting was then carried out with anti-GFP and anti-Myc antibodies. The post-transfer membrane was stained with Ponceau S. **C** and **D**, *In vivo* OsRac1 activation by Pit hydrophobic residues mutants. **C**, Emission ratio images of confocal laser-scanning micrographs of rice protoplasts coexpressing Raichu-OsRac1 and the indicated Pit mutants, or negative control GUS. Scale bars, 5 μm. **D**, Quantification of normalized emission ratios of Venus to CFP. Data are expressed as mean ± standard error (SE) (**$P < 0.01$, $n = 60$).

Wang et al., Figure 5

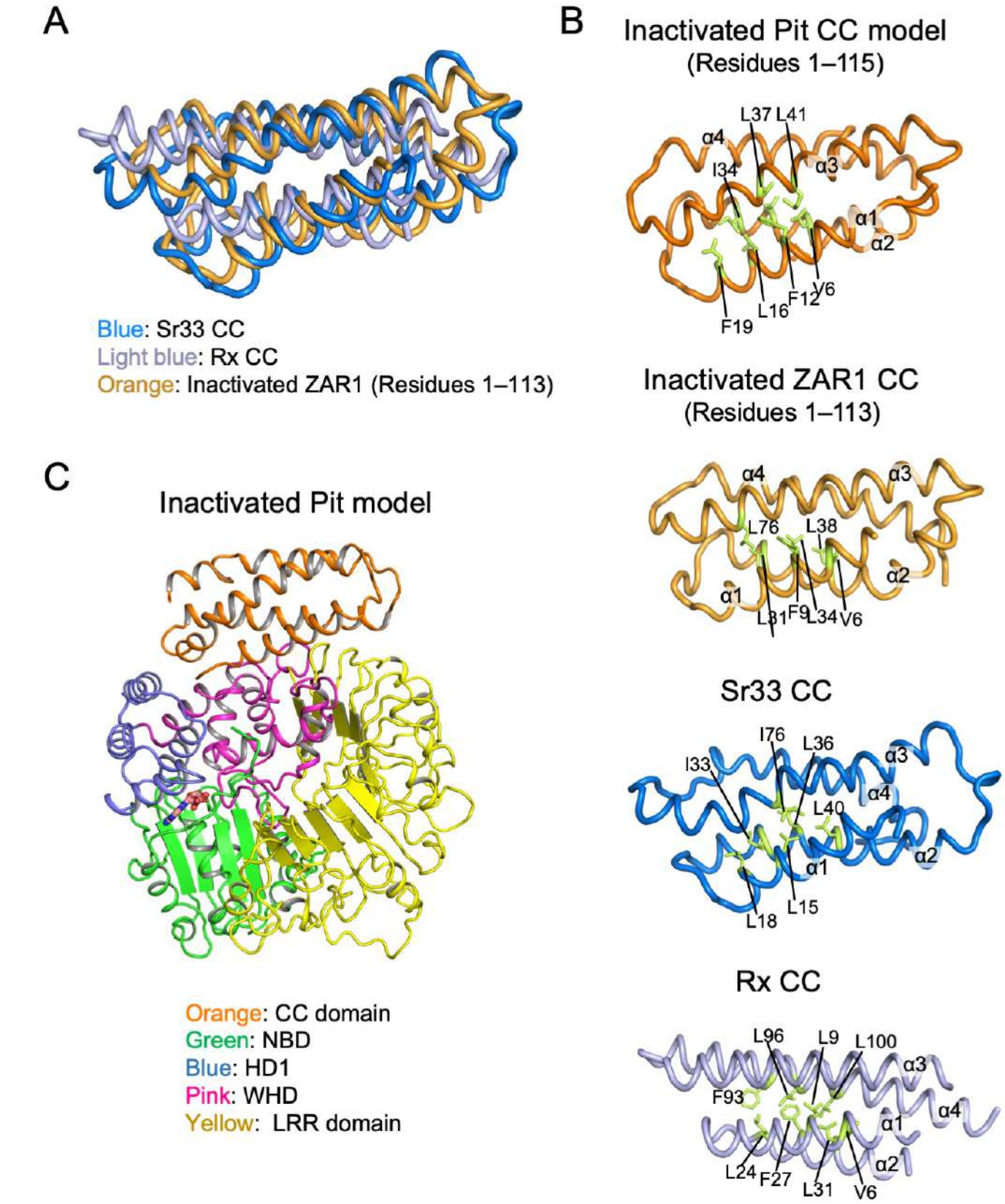

Figure 5. The CC domain of various NLRs

A, The main chains of the CC domain structure of Sr33 (blue, solution NMR condition, Protein Data Bank ID code 2NCG), Rx (light blue, crystal condition, Protein Data Bank ID code 4M70), and inactivated ZAR1 (orange, electron microscopy condition, 6J5W, residues 1-113) were superimposed using PyMOL. **B,** Comparison of conserved hydrophobic residues of Pit (residues 1-115), inactivated ZAR1 (residues 1-113), Sr33, and Rx. The side chains of three key hydrophobic residues in Pit (I34, L37, and L41) and equivalent residues in inactivated ZAR1 1-113 (L31, L34, and L38), Rx (I33, L36, and L40), Sr33 (L24, F27, and L31), as well as the side chains of amino acids thought to be involved in hydrophobic interactions with these three residues, are shown in stick representation. **C,** Model structure and domain composition of full-length Pit, based on inactivated ZAR1 (Protein Data Bank ID code 6J5W), shows the monomeric state. The figure was drawn using PyMOL.

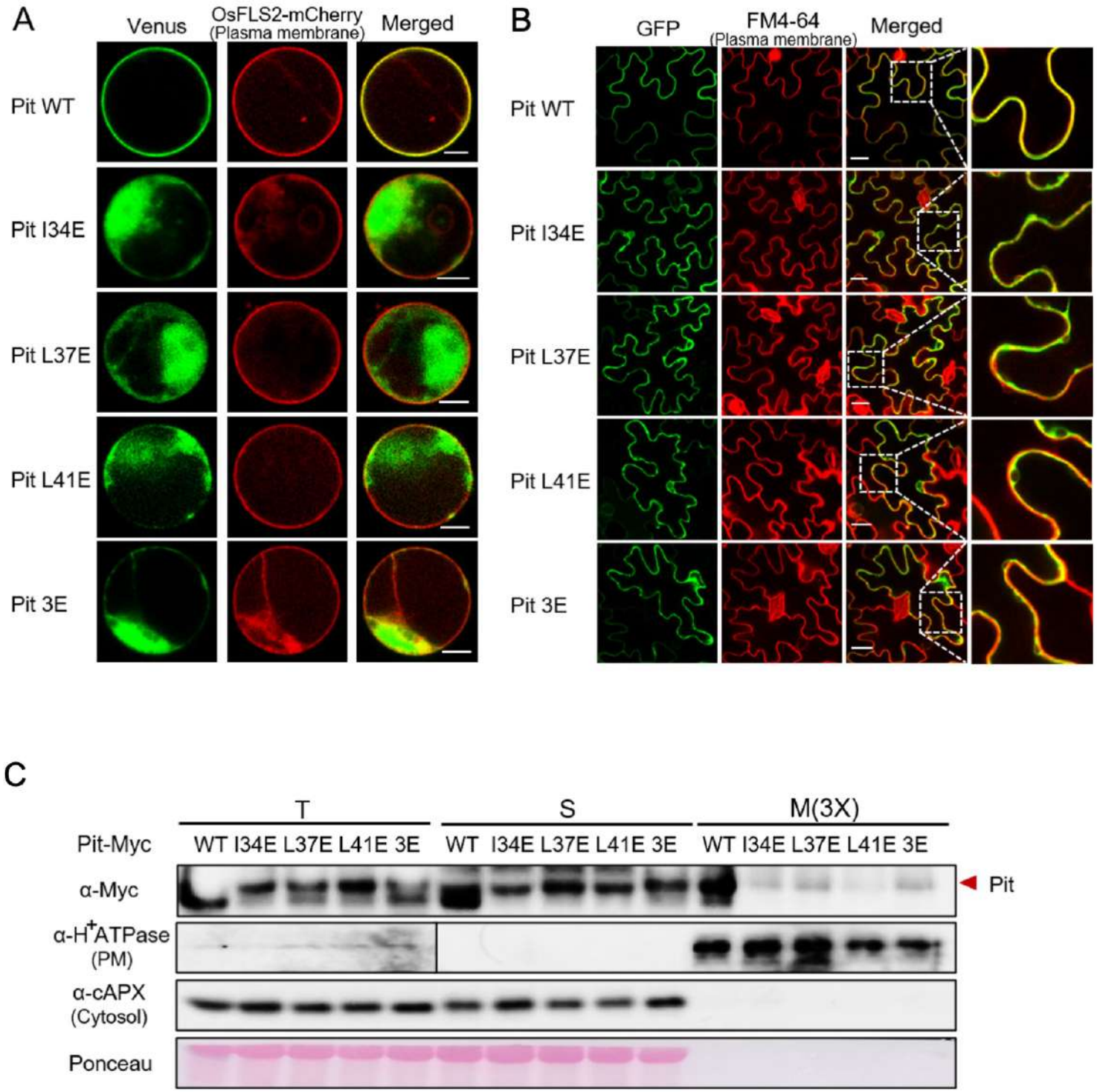

Figure 6. Mutations in the conserved hydrophobic residues of Pit influence its plasma membrane localization
A and **B**, Subcellular localization of Pit mutants in rice protoplasts and *N. benthamiana* leaves. **A**, Rice protoplasts were cotransfected with the indicated *Pit-Venus* mutants and *OsFLS2-mCherry*. Scale bars, 5 μm. **B**, Tobacco leaves were injected with *Agrobacterium* carrying *Pit-GFP* mutants (green) and stained with FM4-64 (red: plasma membrane marker). Enlarged images of the boxed areas are shown in the right panels. Scale bars, 25 μm. **C**, Accumulation of Pit-Myc mutants in tobacco leaves. Immunoblotting was performed with anti-Myc (for Pit mutants), anti-H$^+$ATPase (PM marker), and anti-cAPX (cytoplasm marker) antibodies. T: total extract, S: soluble fraction, M: microsomal fraction. M (3×) indicates three times enrichment relative to T or S. Ponceau staining used as a loading control. These bands are from same blot.

Wang et al., Figure S1

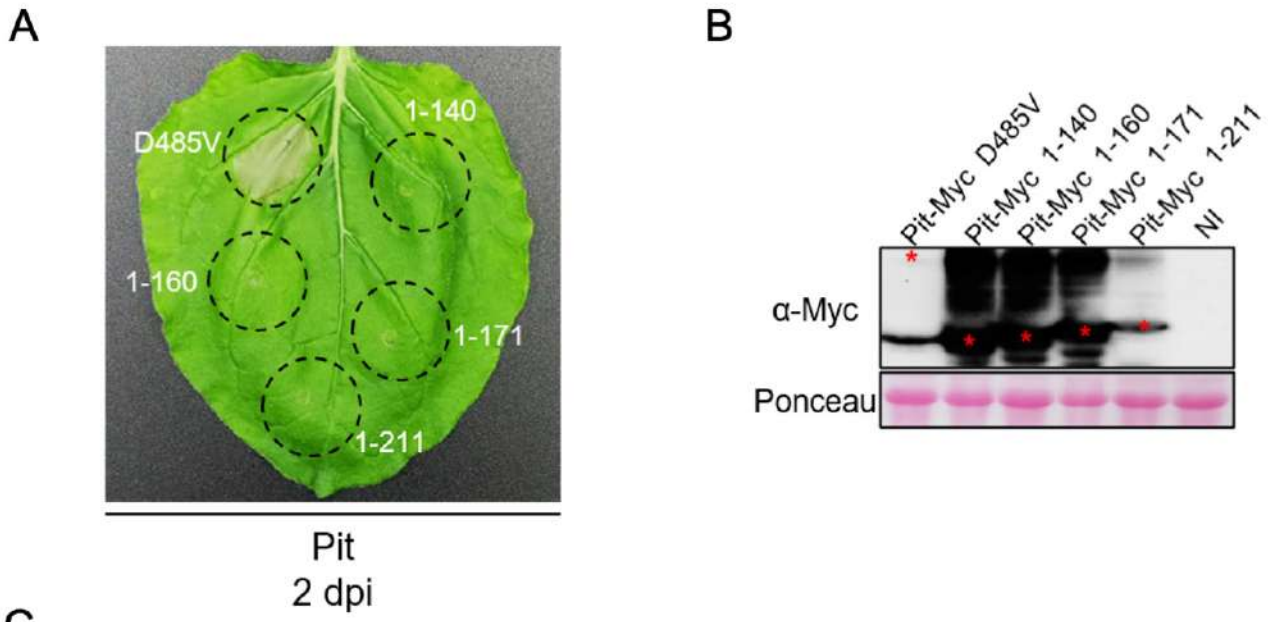

C

```
Pit     MGTV---LDALAWKFLEKLGQLI-EDEVIMTLSVKRGIESLKKNLEFFNA 46
ZAR1    M------VDAVVTVFLEKTLNIL-EEKGRTVSDYRKQLEDLQSELKYMQ- 42
Sr33    MDIVT----GAIAKLIPKLGELLVG-EYKLHKGVKKNIEDLLKELKTMNA 45
Sr50    MNIVT----GAMGSLIPKLGELLMD-EYKLHKRIKKDVEFLKKELESMHA 45
MLA10   MDIVT----GAISNLIPKLGELLTE-EFKLHKGVKKNIEDLGKELDSMNA 45
RPM1    M------ASATVDFGIGRILSVL-ENETLLLSGVHGEIDKMKKELLIMKS 43

Pit     VHEDAEALAMEDPGIDS------WWKNMRDVMFDVDDI-VD--LFMVHSQ 87
ZAR1    SFLKD----AERQKRTNETLRTLVAD-LRELVYEAEDILVDCQL--ADGD 85
Sr33    ALIKI----GEVPPDQLDSQDKLWADEVRELSYVIEDA-VDKFLVRVHG- 89
Sr50    ALIKV----GEVPRDQLDRQVKLWADEVRELSYNMEDV-VDKFLVRVDGD 90
MLA10   ALIKI----GEVPREQLDSQDKLWADEVRELSYVIEDV-VDKFLVQVDG- 89
RPM1    FLEDTHKHGGNGSTTTTTQLFQTFVANTRDLAYQIEDI-LDEFGYHIHG- 91

Pit     KLLLPPRPVCCNQPLFSSFAKFSFD------HMIAKRIDNINEKFEEIKM 131
ZAR1    DGNEQRSSNAWLSRLHPARVPLQYKKSK-RLQEINERITKIKSQVEPYFE 134
Sr33    --VEPDDNTNGFKGLMKRTTKL-LKKVV-DKHGIAHAIKDIKKELQEVAA 135
Sr50    GIQQPHDNSGRFKELKNKMIGL-FKKGR-NHHRIADAIKEIKEQLQEVAA 138
MLA10   --IKSDDNNNKFKGLMKRTTEL-LKKVK-HKHGIAHAIKDIQEQLQKVAD 135
RPM1    ----------YRSCAKIWRAFHFPRYMWARHSIAQKLGMVNVMIQSISD 130

Pit     NKEMFGL-------ERTNRQQIQITIVDRSQTSPVD----------ELEV 164
ZAR1    ----------------------FITPSNVGRDNGTDRWSSPVY--DHTQV 160
Sr33    RRDRNK----------------FDGIASIPTEAIDPRLRALY-IEAAEI 167
Sr50    RRDRNK----------------VAVPNPMEPITIDPCLRALY-AEATEI 170
MLA10   RRDRNK----------------VFVPHPTRTIAIDPCLRALY-AEATEI 167
RPM1    SMKRYYHSENYQ--------AALLPPIDDGDAKWVNNISESSLFFSENSL 172
```

Figure S1. The CC domain of Pit is not sufficient to induce cell death

A, Cell death phenotypes induced by transient expression of Pit N-terminal deletion mutants in *N. benthamiana*. Photos were taken at 2 dpi. The circles indicate the infiltrated regions. Numbers indicate amino acid boundaries of Pit mutants. **B,** Myc-tagged Pit mutants were transiently expressed in *N. benthamiana* leaves. After 2 days, the total proteins of infiltrated leaves were extracted for immunoblotting with anti-Myc antibody. NI indicates non-infiltrated leaves. The post-transfer membrane was stained with Ponceau S and used as an internal control. **C,** protein sequence alignment among the CC domain of R proteins. Each background color indicates minimal region of NLRs required for cell death induction or oligomerization.

Wang et al., Figure S2

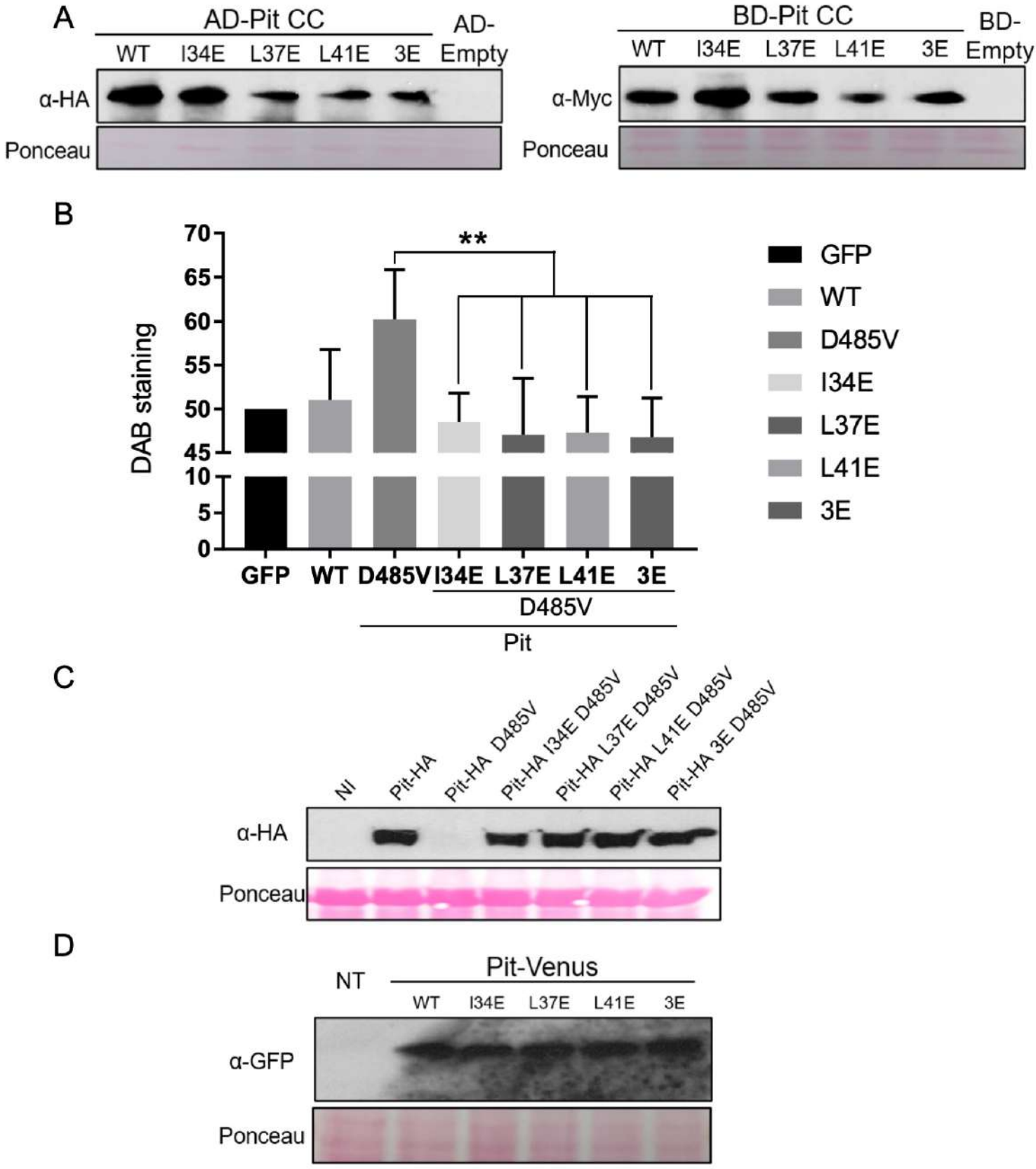

Figure S2. Effect of conserved hydrophobic residue mutations on Pit signaling

A, Protein expression of Pit CC WT and mutants in Y2HGold yeast cells. Anti-HA and anti-Myc antibodies were used for western blot to detect baits and preys, respectively. The post-transfer membrane was stained with Ponceau S. **B**, Quantitative analysis of the effect of I34, L37, and L41 mutation on Pit D485V-induced ROS production in *N. benthamiana*. Bars indicate DAB staining intensity relative to that observed after infiltration with negative control GFP. Data are expressed as mean ± standard error (SE) (**: $P < 0.01$; $n = 10$). Relative intensity of DAB staining (GUS=50) is shown. **C**, HA-tagged Pit mutants were transiently expressed in *N. benthamiana* leaves. After 2 days, the total proteins of infiltrated leaves were extracted for immunoblotting with anti-HA antibody. NI indicates non-infiltrated leaves. The post-transfer membrane was stained with Ponceau S and used as an internal control. **D**, Venus-tagged Pit mutants were transiently expressed in rice protoplasts. After 14 h, total protein was extracted with SDS loading buffer, and western blotting was then carried out with anti-GFP antibody. NT indicates a non-transformed sample. The post-transfer membrane was stained with Ponceau S.

Wang et al., Figure S3

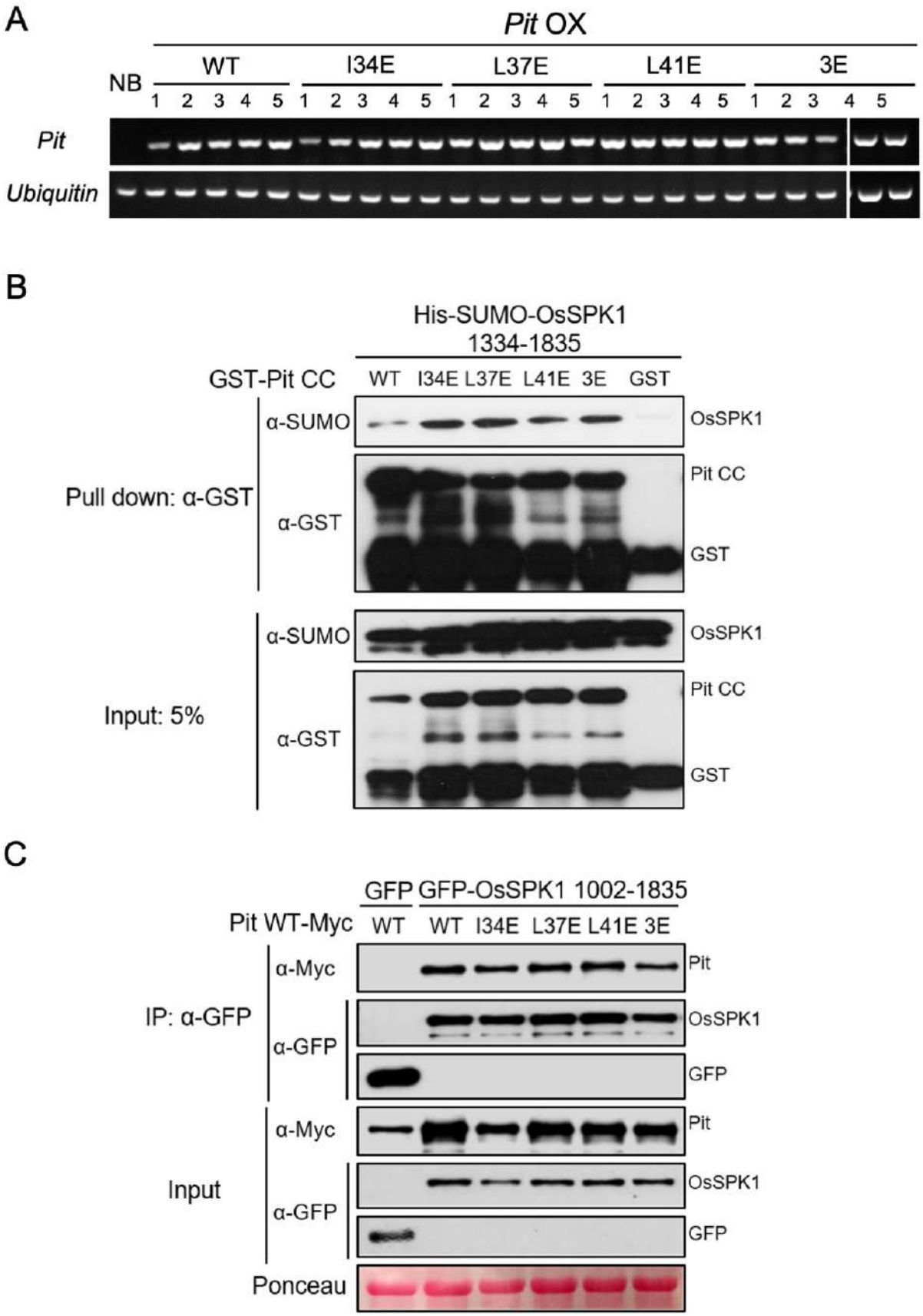

Figure S3. Three hydrophobic residues in the Pit CC domain are not necessary for binding to OsSPK1

A, Transcript levels of exogenous *Pit* WT and *Pit* mutants were measured by RT-PCR. Numbers indicate independent transgenic lines. *Ubiquitin* was used as an internal control. **B,** *In vitro* binding assay between Pit CC mutants and OsSPK1. Purified GST or GST-tagged Pit CC mutants immobilized on Sepharose were incubated with His-SUMO-tagged OsSPK1 (amino acids 1334–1835). After washing, the bound proteins were eluted by addition of SDS loading buffer. Anti-GST and anti-SUMO antibodies were used for subsequent western blotting analysis. **C,** Co-IP to analyze the interaction in *N. benthamiana* between OsSPK1 (amino acids 1002–1835) and full-length Pit with mutations in three conserved hydrophobic residues. Total protein extract was immunoprecipitated with anti-GFP antibody, and western blotting was then carried out with anti-GFP and anti-Myc antibodies. The post-transfer membrane was stained with Ponceau S.

Wang et al., Figure S4

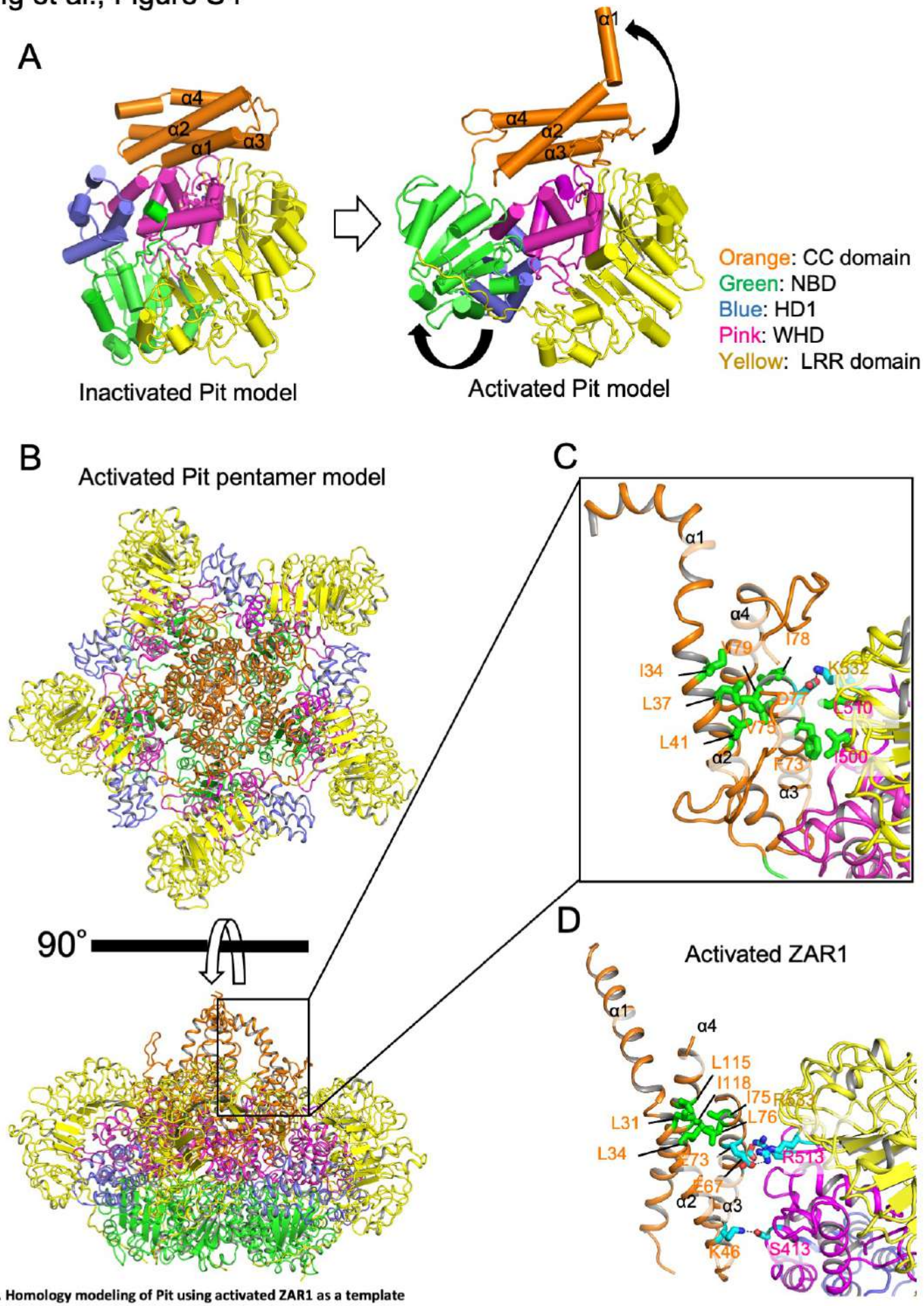

Figure S4. Homology modeling of Pit using activated ZAR1 as a template

A, Comparison of the Pit structure models based on the active and inactive ZAR1. The structure models of Pit are based on the structures of inactivated ZAR1 (Protein Data Bank ID code 6J5W) and activated ZAR1 (Protein Data Bank ID code 6J5T). Conformational changes (black arrows) between the Pit structure models based on the active and inactive ZAR1 occur around the hinge linking the HD domain (blue) and WHD domain (pink) of Pit and also at the α1 helix of the CC domain (orange). **B,** Structure model of the Pit pentamer based on the activated ZAR1. The extreme N-terminal α1 helix of the Pit pentamer may be required for the plasma membrane association of Pit. The CC, NBD, HD1, WHD, and LRR domains are shown in orange, green, blue, pink, and yellow, respectively. **C,** Hydrophobic interactions among α2 (I34, L37, and L41), α3 (F73, V75, I78, and V79), and WHD domain (I500 and L510) in the Pit pentamer structure model based on the activated ZAR1 are shown. Residues that may be important for hydrophobic interactions in Pit function are shown in green, and hydrogen-bonded side chains are shown in light blue. **D,** Comparison of the interaction around α1 of the activated ZAR1 structure (Protein Data Bank ID code 6J5T) and the Pit oligomer structure model based on the active ZAR1. Residues involved in hydrophobic interaction around α1 are shown in green, and hydrogen-bonded side chains are shown in light blue. The figure was drawn using PyMOL.

Wang et al., Figure S5

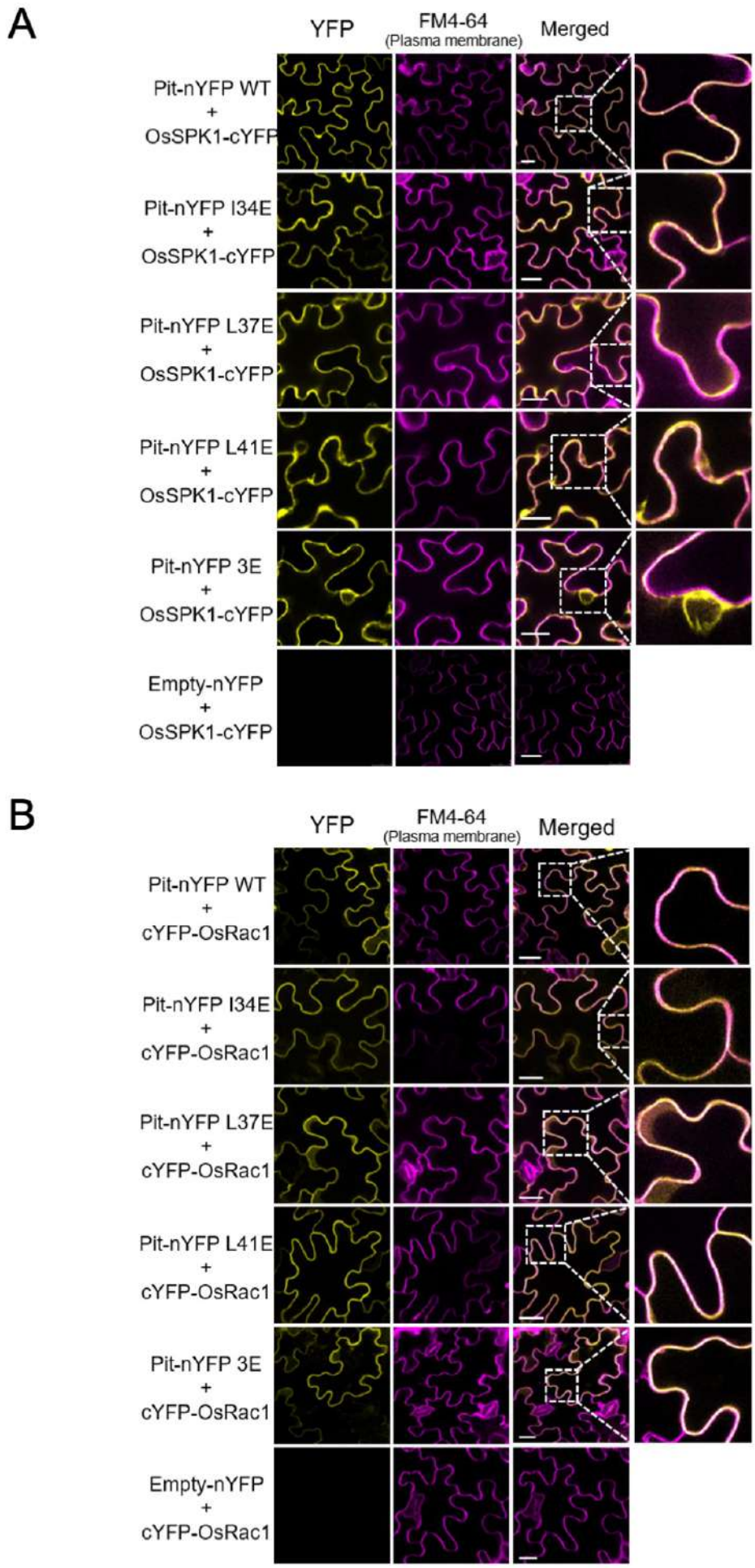

Figure S5. Subcellular-interaction locations between Pit mutants and OsSPK1 or OsRac1

A and B, BiFC to detect interactions between Pit hydrophobic residue mutants and OsSPK1 (A) or OsRac1 (B). Expression constructs were transiently expressed in N. benthamiana after agroinfiltration. Empty vector served as a negative control. FM4-64 was used as a plasma membrane marker. Images were captured at 45 h post-infiltration. Enlarged images of the boxed areas in (A and B) are shown in the right panels. Scale bars, 25 μm.

Wang et al., Table S1

Primers for this study	
Primer name	**Sequence (5'-3')**
MgPot2-F	ACGACCCGTCTTTACTTATTTGG
MgPot2-R	AAGTAGCGTTGGTTTTGTTGGAT
UBQ-F	AACCAGCTGAGGCCCAAGA
UBQ-R	ACGATTGATTTAACCAGTCCATGA
PAL1-F	TGAATAACAGTGGAGTGTGGAG
PAL1-R	AACCTGCCACTCGTACCAAG
PBZ1-F	GGTGTGGGAAGCACATACAA
PBZ1-R	GTCTCCGTCGAGTGTGACTTG
Primers for RT-PCR	
Primer name	**Sequence (5'-3')**
Pit OX-F	CTGCACTTTGAATACCATTGGC
Pit OX-R	GGAGAATTTCCAATCTCTGTAATCTAA
Ubiquitin-F	CCAGGACAAGATGATCTGCC
Ubiquitin-R	AAGAAGCTGAAGCATCCAGC
Primers for mutagenesis	
Primer name	**Sequence (5'-3')**
Pit I34E-R	TCTTCAGGCTCTCCTCACCCCTTTTCACACTTAATG
Pit L37E-F	GTATTGAGAGCGAGAAGAAAAATCTGGAATTC
Pit L37E-R	AGATTTTTCTTCTCGCTCTCAATACCCCTTTTC
Pit L41E-F	AGCCTGAAGAAAAATGAGGAATTCTTCAACGCTG
Pit L41E-R	AGCGTTGAAGAATTCCTCATTTTTCTTCAGGCTCTC
Pit 3E-F	TGAAAAGGGGTGAGGAGAGCGAGAAGAAAAATGAGGAATTCTTCAACGCTGTTC
Pit 3E-R	TGAAGAATTCCTCATTTTTCTTCTCGCTCTCCTCACCCCTTTTCACACTTAATG

Supplementary Figure 1 for the reviewers

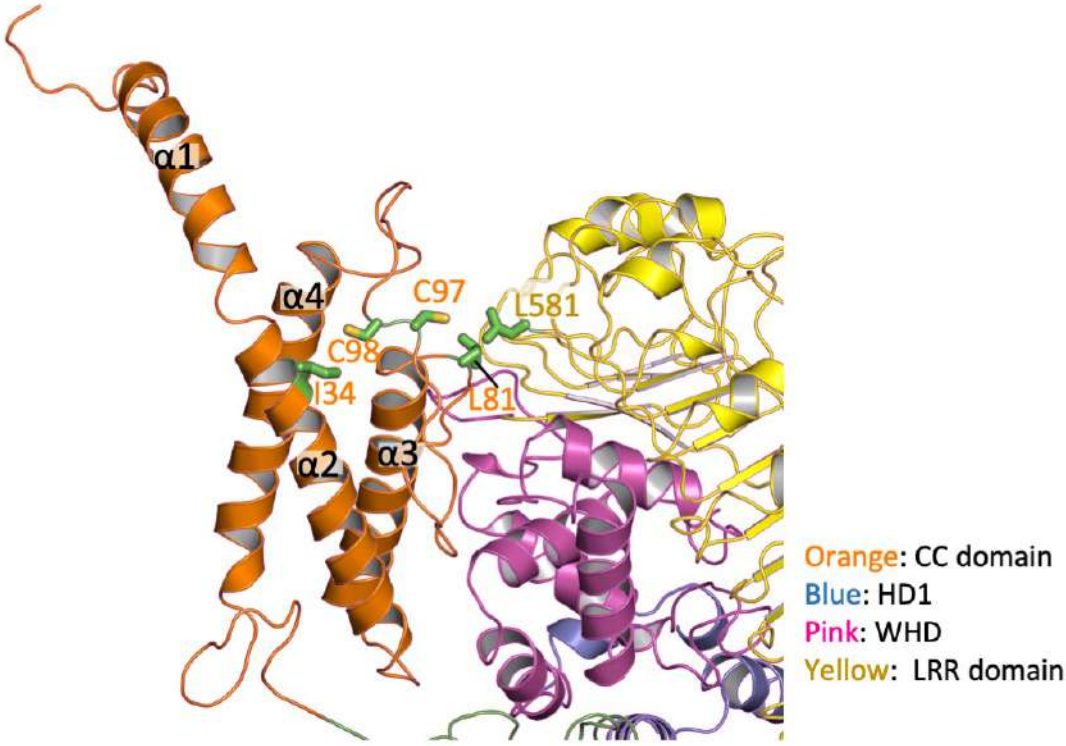

Figure S1 for the reviewers. Effects of conserved hydrophobic residue mutations on Pit palmitoylation modification

Hydrophobic interactions among I34 (α2), L81 (loop between α3 and α4), C98, C99 (Palmitoylation site), and L581 (LRR domain) in the Pit pentamer structure model based on the active ZAR1 are shown. Residues that may be important for hydrophobic interactions by the palmitoylation in Pit function are shown in green. The figure was drawn using PyMOL.

Supplementary Figure 2 for the reviewers

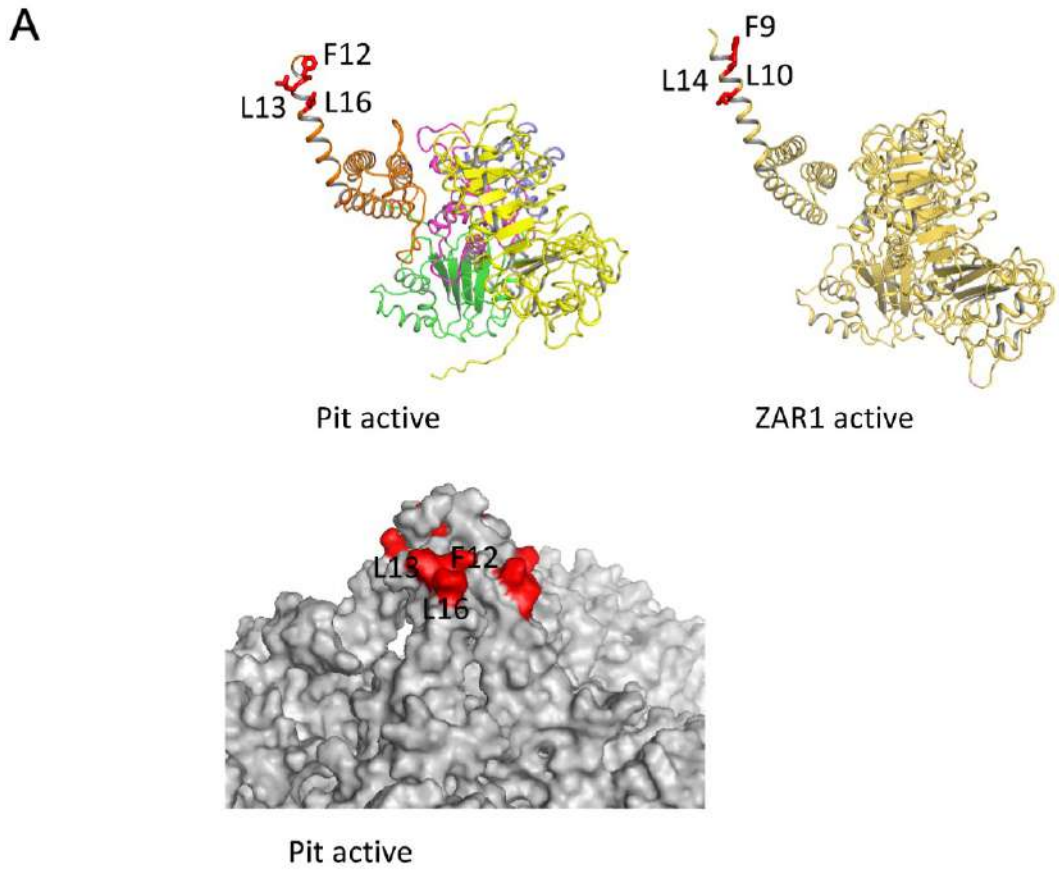

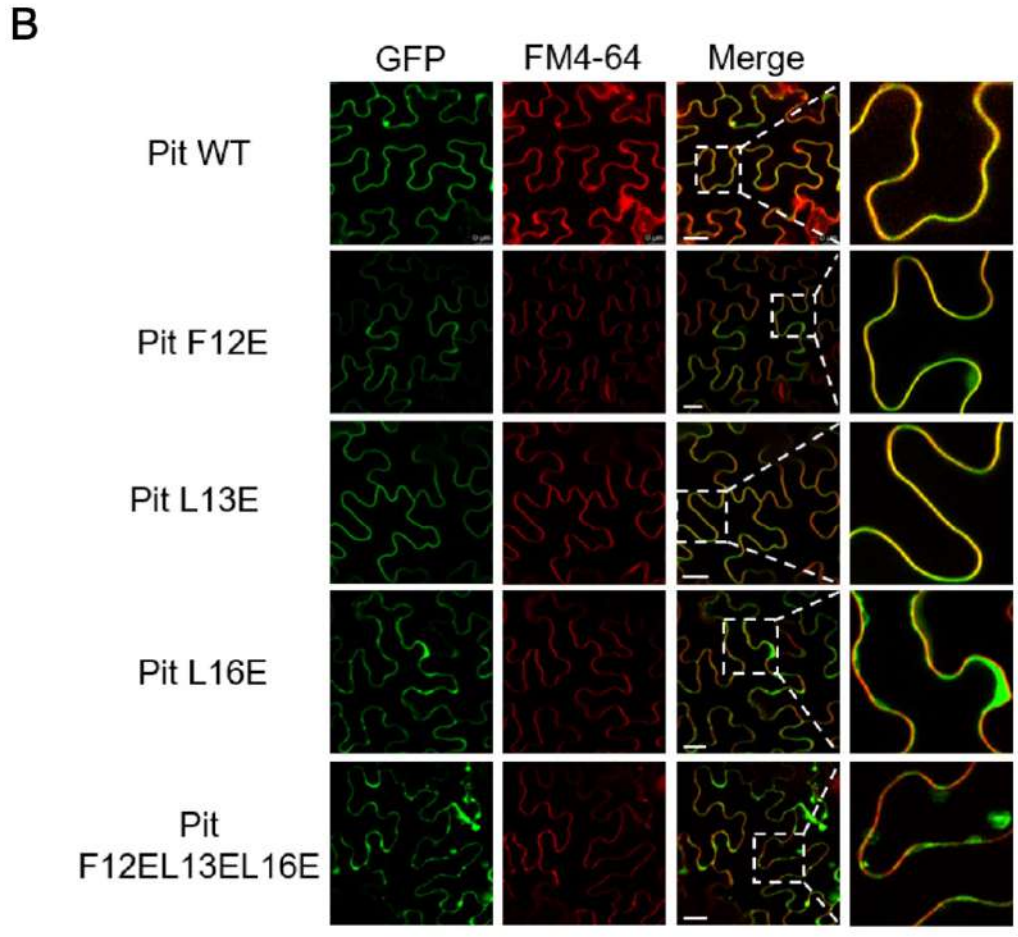

Figure S2 for the reviewers. Pit α1 helix plays a role in the plasma membrane localization

A, The position of F12, L13, and L16 in Pit correspond to F9, L10, and L14 in ZAR1 are shown. The figure was drawn using PyMOL. **B**, Tobacco leaves were injected with *Agrobacterium* carrying *Pit-GFP* mutants (green) and stained with FM4-64 (red: plasma membrane marker). Enlarged images of the boxed areas are shown in the right panels. Scale bars, 25 μm.

Supplementary Figure 3 for the reviewers

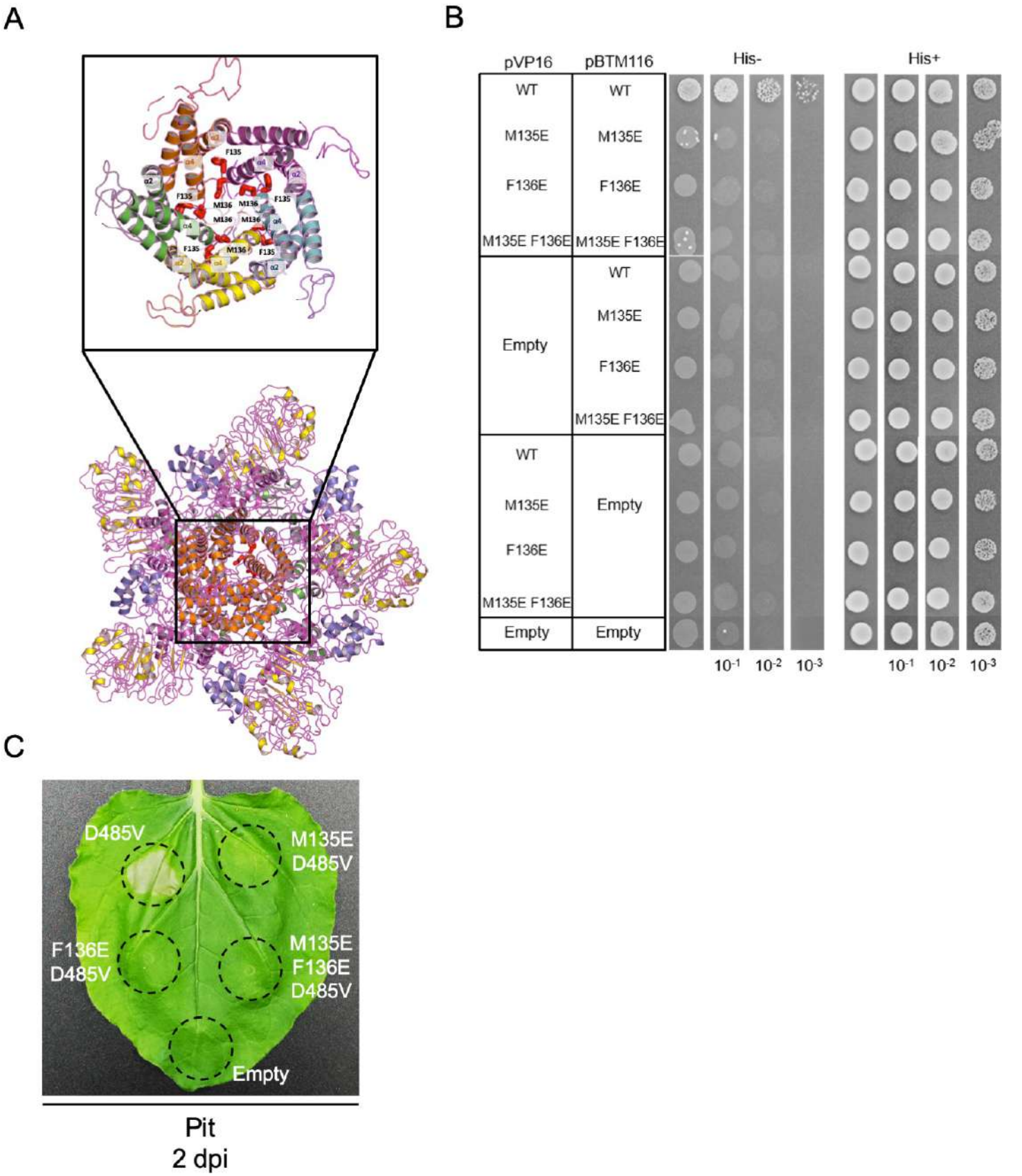

Figure S3 for the reviewers. M135 and F136 contribute to Pit oligomerization and cell death activity

A, The position of M135 and F136 in the Pit pentamer structure model based on the active ZAR1 are shown. M135 and F136 residues are shown in red sticks. Each CC domain of Pit's pentamer was color coded. The figure was drawn using PyMOL. **B**, Yeast two-hybrid assay to test self-association of Pit CC mutants. Growth of yeast cells coexpressing VP16-NLS or LexA fused with the CC domain of Pit on selective medium (-His) represents a positive interaction. 10^{-1}, 10^{-2}, and 10^{-3} indicate dilution ratio. **C**, Cell death phenotypes induced by transient expression of Pit mutants in *N. benthamiana*. Photos were taken at 2 dpi. The circles indicate the infiltrated regions.

Supplementary Figure 4 for the reviewers

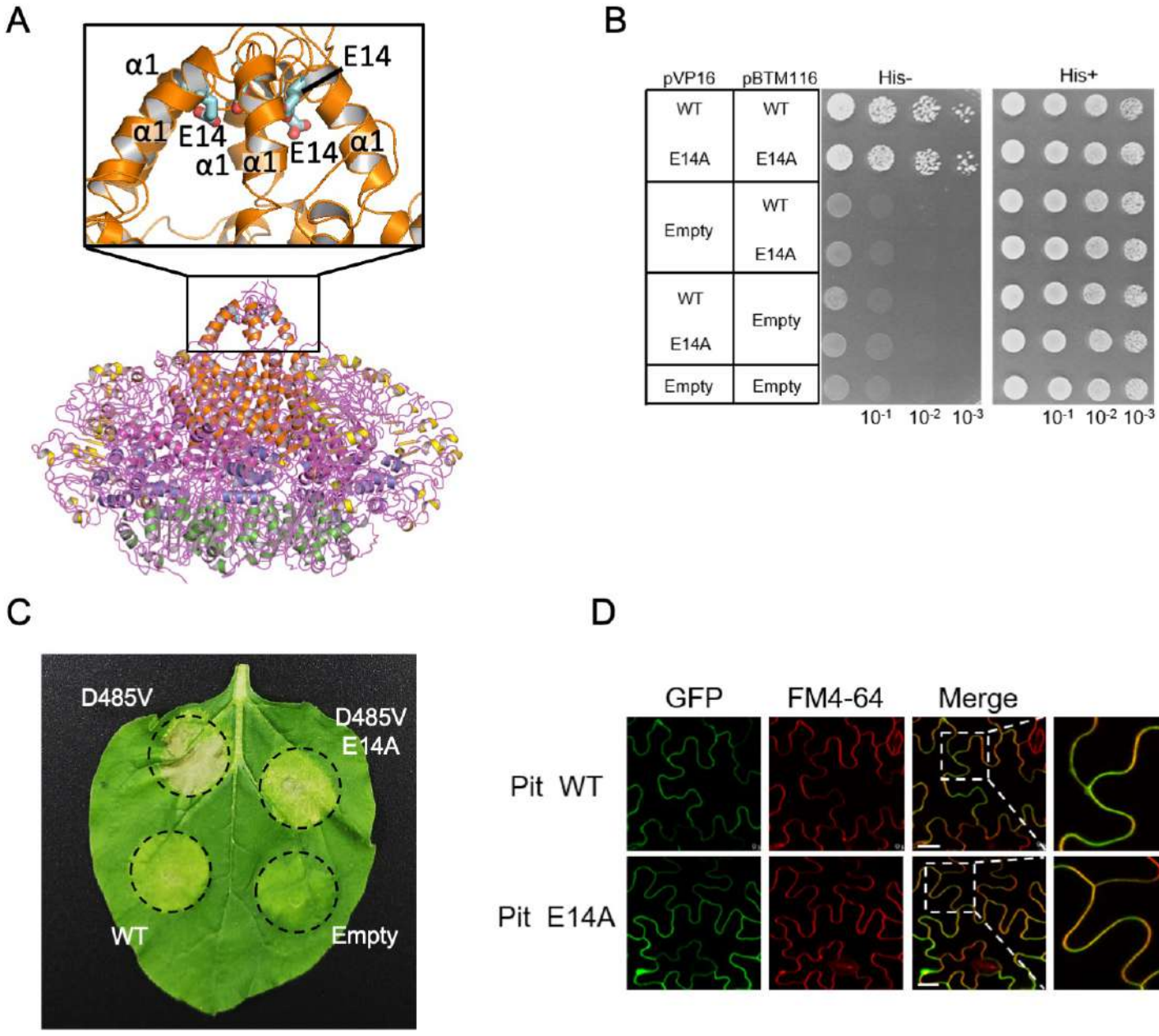

Figure S4 for the reviewers. M135 and F136 contribute to Pit oligomerization and cell death activity

A, The position of E14 in the Pit pentamer structure model based on the active ZAR1 are shown. E14 residues are shown in sticks. The figure was drawn using PyMOL. **B**, Yeast two-hybrid assay to test self-association of Pit CC mutants. Growth of yeast cells coexpressing VP16-NLS or LexA fused with the CC domain of Pit on selective medium (-His) represents a positive interaction. 10^{-1}, 10^{-2}, and 10^{-3} indicate dilution ratio. **C**, Cell death phenotypes induced by transient expression of Pit mutants in *N. benthamiana*. Photos were taken at 2 dpi. The circles indicate the infiltrated regions. **D**, Tobacco leaves were injected with Agrobacterium carrying Pit-GFP WT and E14A (green) and stained with FM4-64 (red: plasma membrane marker). Enlarged images of the boxed areas are shown in the right panels. Scale bars, 25 μm.